SURFACEFUNCTIONALIZATION OF MHz-RANGE SILICON RESONATORS: CONTROLLING MECHANICALENERGY DISSIPATION AND ADDING CHEMICAL FUNCTIONALITY

A Dissertation

Presented to the Faculty of the Graduate School

Of Cornell University

In Partial Fulfillment of the Requirements for the Degree of

Doctor of Philosophy

by

Debodhonyaa Sengupta

August 2008

©2008 Debodhonyaa Sengupta

SURFACE FUNCTIONALIZATION OF MHz-RANGE SILICON RESONATORS: CONTROLLING MECHANICAL ENERGY DISSIPATION AND ADDING CHEMICAL FUNCTIONALITY

Debodhonyaa Sengupta, Ph. D.

Cornell University 2008

The surface chemistry of silicon resonators plays an important role in mechanical energy dissipation. Significantly higher quality factors are observed for methyl-terminated-MHz-frequency silicon oscillators as compared to similar resonators terminated with longer alkyl moieties. Megahertz-frequency silicon micromechanical torsional resonators were coated with mixed monolayers consisting of methyl groups with a small admixture of functional moieties. Infrared absorption spectroscopy and X-ray photoelectron spectroscopy were used to characterize the functionalized surfaces. Resonators terminated with mixed acetal/methyl monolayers had very high quality factors. In contrast, when the acetal moiety was converted to an aldehyde using standard deprotection chemistries in both aqueous and organic media, a dramatic decrease in resonator quality was observed. Resonators terminated with a mixture of methyl and butenyl moieties were found to have high quality factors than those observed for methyl-terminated resonators. Furthermore, the terminal double bond on the butenyl moiety was reacted with the terminal double bond on ethyl 10-undecenoate molecule via olefin cross-metathesis, resulting in ester-terminated resonators. The resulting quality factor of the resonators was found to be acceptably high. Thus, a successful method for termination of resonators with reactive functional groups while maintaining high quality factor was established.

BIOGRAPHICAL SKETCH

Debodhonyaa Sengupta was born in the East Indian city of Calcutta on March 20, 1979. Her academic training started at the renowned La Martiniere for Girls School in Calcutta, which she attended for fifteen years, as her mother had before her. During her time at La Martiniere she excelled in academics as well as extra-curricular activities, notably passing the Grade 8 examination in Pianoforte Performance with the Royal Schools of Music, London in 1996.

Upon graduating from La Martiniere she joined the Department of Chemistry at Miranda House College for Women, University of Delhi. During her years as an undergraduate in the field of chemistry, Debodhonyaa spent her summers working at various leading scientific institutions in the country, including the Indian Institute of Technology in Kanpur, the Indian Association for the Cultivation of Science in Calcutta, and the Center for Biochemical Technology in Delhi. Short-term research projects at these institutes introduced her to the exciting life of a research scientist.

In the summer of 2002, Debodhonyaa moved from hot and sweltering Delhi to the much cooler clime of Ithaca, NY to embark on a graduate career in Chemistry. Debodhonyaa's time at Cornell has been a learning experience. She has especially benefited from the training provided by Prof. Melissa A. Hines, not only as a scientist but also as a speaker and writer. This training will be invaluable as she embarks on her legal career. Although she enjoined the academic experience at Cornell, the five cold winters of Ithaca made her want to move to a warmer city.

Thus, in August 2007, Debodhonyaa moved to Washington D. C. with Boots and Tess. Stepping into the real world, she joined Sughrue Mion, PLLC, as a Technical Specialist, specializing in patent prosecution and litigation related to the chemical and pharmaceutical arts. Starting in August 2008, Debodhonyaa will go back

to school part-time, to earn a Juris Doctor degree from the George Washington University Law School.

Some day in the future, Debodhonyaa would like to be able to travel the world, pass the F.R.S.M. examination in pianoforte performance, adopt a (or a few) dogs, and maybe even learn how to ride a bicycle.

ACKNOWLEDGMENTS

Many years ago, when I embarked on an academic career in the sciences, I had no idea that it would last this long and be as exciting as it has turned out to be. The person most responsible for my success is Prof. Melissa Hines. Without Melissa's guidance and tutelage I would not have made it this far.

Along the way there have been many teachers who have influenced and shaped the trajectory of my academic life – Mrs. Reina Banerjee, Dr. Bani Roy, Dr. Amrita T. Sheikh, my teachers at La Martiniere and the chemistry faculty at Miranda House – to them I owe my heartfelt gratitude.

Simon Garcia, Yu Wang, Josh Henry, Hailing Bao, Marc Faggin, Ian Clark, Amy Richter, Ankush Gupta, Brandon Aldinger – the "hard working" members of the Hines lab – thank you for lending a helping hand where necessary, especially towards the end of my time at Cornell. A special thank you to Ian and Amy for your help.

A special Thank You to Jamie Lee Cohen, without whom my years in Ithaca would have been a lot less tolerable.

There are many who did not have a direct hand in shaping my graduate career, or this dissertation, but have been a part of this long journey right from the very beginning, – Haimanti Nag, Namrata Mitra, Upal Kusari; while there are others who have been an integral part of the long and arduous year that it took to finish writing this dissertation – Tom Hunter, Mike Jones, and Chris Bezak. To all of you – Thank you.

Finally, I would like to thank my parents, Saumya and Debjani Sengupta for all their support through the years.

TABLE OF CONTENTS

LIST OF FIGURES

Chapter 1

Chapter 2

Chapter 3

Chapter 4

Chapter 1

Introduction

1.1 Micromechanical Devices as Sensors

Micromechanical devices have found applications in fields as wide ranging as picojoule and submillisecond calorimetry [1], high frequency standards [2], and dynamic force microscopy [3]. One emerging field that has generated a significant amount of interest is the use of micromechanical devices in chemical and biological sensors. For example, silicon nitride oscillators coated with a thin gold film have been used to detect mercury vapor in air [4]. In this application, the adsorption of an analyte is detected by a change in the resonant frequency of a vibrating element, such as a cantilever. This change in frequency is a result of a small change in the mass of the device. According to Hooke's Law, the frequency, f, of a harmonic oscillator is related to its mass, M, by

$$f = \frac{1}{2\pi}\sqrt{\frac{k}{M}}, \tag{1.1}$$

where k is the spring constant of the oscillator.

If the mass of the resonator is increased by an infinitesimal amount ∂M, the resonant frequency decreases by an amount ∂f that is given by

$$\partial f = -\frac{1}{4\pi} k^{1/2} M^{-3/2} \partial M . \tag{1.2}$$

Equations (1.1) and (1.2) can be combined to obtain an expression for the fractional change in frequency,

$$\frac{\partial f}{f} = -\frac{1}{2}\frac{\partial M}{M}. \tag{1.3}$$

In other words, the fractional change in frequency is proportional to the fractional change in mass.

1.2 The Importance of High *Q*

The sensitivity of a resonant mass sensor is determined by the smallest change in resonant frequency that can be accurately measured. This quantity is in turn determined by the quality factor, Q, of the resonator. In layman's terms, the quality factor of a resonator is approximately the number of vibrations that a resonator will undergo after an impulsive excitation before coming to a rest. High-Q resonators have low rates of mechanical energy dissipation and oscillate many times before coming to rest. Conversely, low-Q resonators are highly dissipative. Mathematically, the Q of a resonator is defined by

$$Q = \frac{2\pi \times E}{\Delta E}, \tag{1.4}$$

where E is the total energy stored in the resonant device, and ΔE is the mechanical energy loss per cycle of oscillation. The Q for resonant devices is also related to the relative change in frequency $\partial f/f$, the Q being inversely proportion to $\partial f/f$. Therefore, resonators with higher quality factors are more sensitive to small additive masses as compared to resonators with lower quality factors. (The relation between the relative change in resonant frequency and absorbed mass was discussed in Sect. 1.1.)

The effect of Q on mass sensitivity can be understood by comparing two resonators with identical frequencies but different quality factors, as shown in Fig 1.1. The left hand side of the figure follows the displacement of loaded and unloaded resonators as a function of time. The most dramatic difference between the resonators is that the motion of the low Q resonator decays much more rapidly with time than

that of the high Q resonator (irrespective of loading). There is also a more subtle difference. At early times, the displacement of the loaded and unloaded devices are nearly identical, irrespective of the Q of the devices. It is only after long periods of time that the small loading leads to a noticeable phase lag. Interestingly, this lag is only observable in the high Q device. The rapid decay of the low Q device damps the motion before the lag is noticeable. As a result, the high Q device is more sensitive to mass changes than the low Q device.

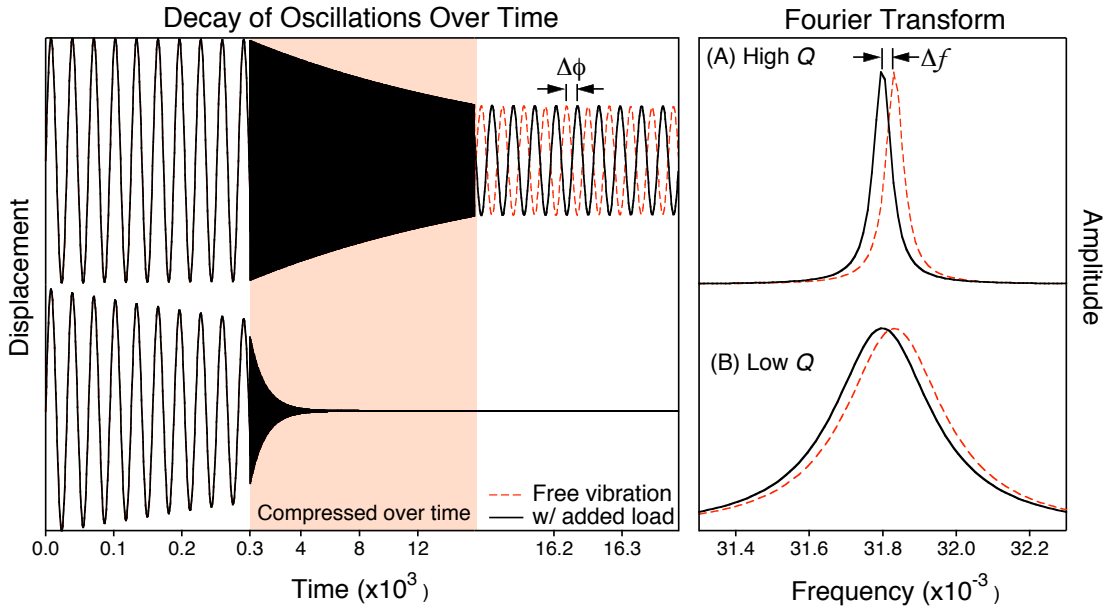

Figure 1.1 The behavior of two resonators with identical frequencies but different quality factors is compared. The left side of the figure shows the oscillation of the loaded and unloaded resonators over time. The right side of the figure shows the Fourier transform of the displacement for the two resonators. The top half of both the figures corresponds to a resonator with a high quality factor, whereas the bottom half corresponds to a resonator with lower quality factor.

This phenomenon can also be observed in the frequency domain. In the right side of Fig. 1.1, the Fourier transform of the displacement of the high Q device is sharp and narrow, whereas that of the low Q device is much broader. The change in frequency due to the added mass is identical for both devices, but the higher

mechanical energy dissipation in the low Q device, and hence the broader peak, makes the quantification of this change more difficult.

Albrecht and coworkers, in a seminal paper discussing the sensitivity of force microscopy [5], showed that

$$(\delta\omega)^2 = \frac{\omega_0 k_B T B}{k_L Q < z_{osc}^2 >} \tag{1.5}$$

where $\delta\omega$ is the minimum detectable frequency change, ω_0 is the resonant frequency, k_BT is the thermal energy at the ambient temperature, B is the measurement bandwidth measured in Hz, k_L is the force constant of the lever, $<z_{osc}^2>$ is the mean square amplitude of the driven cantilever, ($k_L<z_{osc}^2>$) is the oscillator energy and Q is the quality factor. The experiments in Albrecht *et al.* used a low-noise displacement sensor and an all fiber interferometer, so that the thermal vibration of the devices was the main source of frequency noise.

Ekinci and coworkers [6] subsequently investigated the mass sensitivity of resonant detectors. Thermomechanical noise in resonant devices imposes a fundamental limit on mass measurements. Therefore, in characterizing mass sensitivity of a resonant device, it becomes necessary to include thermal contributions. The mass sensitivity, or the minimum detectable mass, δM, for a doubly clamped harmonic silicon oscillator is given by

$$\delta M \approx 2M_{eff}\left(\frac{E_{th}}{E_c}\right)^{1/2}\left(\frac{\Delta f}{Q\times\omega_0}\right)^{1/2}, \tag{1.6}$$

where M_{eff} is the mass of the resonator, E_{th}= k_bT is the thermal energy of the resonant device, E_c= $k_L<z_{osc}^2>$ is the maximum drive energy, ω_0 is the resonant frequency, and Δf is the measurement bandwidth. This relationship assumes that $Q \geq 1$ – a reasonable assumption for micron-scale silicon resonators, which typically have $Q \geq 10^3$. This analysis also assumes that the adsorbed mass has no effect on the mechanical

properties of the device – an assumption that will be shown to be inapplicable for some of the devices studied here. As in Albrecht *et al.* [5], in their analysis Ekinci *et al.* assumes that thermal fluctuations are the dominant source of noise.

The above experiments demonstrate that minimum detectable change in frequency and the minimum detectable change in mass are proportional to $1/\sqrt{Q}$.

1.3 Improving the Quality Factor of Micromechanical Resonators

Mechanical energy dissipation in micromechanical resonators can be attributed to many different pathways, including bulk losses, viscous-drag losses and clamping losses. In general, theses losses are additive. Viscous-drag induced dissipation is important at atmospheric pressure and can be reduced by operating devices at pressures lower than 10^{-3} Torr given typical micromechanical oscillator dimensions [7]. Clamping losses are due to the transfer of energy from the resonant device to the bulk through the support structure. The effect of clamping losses has been studied by Mihailovich *et al* [8]. Mechanical dissipation in bulk materials occurs as a result of phonon-phonon interaction, thermoelastic dissipation, dissipation due to structural defects, and dissipation due to free electrons [9]. In general, crystalline semiconductors such as silicon have low bulk losses.

Many previous researchers have noted a puzzling decrease in Q with decreasing resonator size [8, 10-12]. For example, Esashi and coworkers showed that annealing ultra-thin silicon cantilevers at 1000°C for 30 sec resulted in a two-fold increase in Q; however, the Q subsequently decreased when these cantilevers were left in a UHV chamber for 24 hours. The decrease in Q was attributed to a modification of the surface rather than the annealing process [11]. Esashi and coworkers further demonstrated that after treatment, the Q values were independent of cantilever width

but were proportional to the thickness of the cantilever, which they attributed to the dominance of surface dissipation. Esashi's research demonstrated that scaling down the size of the cantilever does not necessarily mean suppression of the Q factor, and that higher Q factor and thus higher force sensitivity are achievable through annealing. Mihailovich and MacDonald demonstrated that etching processes used in resonator fabrication damages the side-walls, thus affecting Q. The Q can be almost doubled by oxidizing the surface after fabrication, which was attributed to the consumption of the damaged silicon layer during the oxidation process [8]. Finally, Carr *et al.* demonstrated that an increase in surface-to-volume ratio is correlated with a decrease in Q [12]. These experiments suggest that surface-related dissipation is an important mechanism for energy dissipation.

To quantify mechanical energy dissipation at surfaces, previous researchers systematically varied the chemistry at the surface of identical MHz-frequency resonators. For example, when a single monolayer of H atoms on the surface of a 5-μm-wide, 250-nm-thick silicon resonator was replaced with 13 Å of silicon dioxide, energy dissipation was increased by 70% [13]. A rather surprising result was the scaling observed in these devices – mechanical energy dissipation was shown to scale with the surface area of the device, not just the surface area in strained regions [13]. Could surface functionalization prevent this surface-induced mechanical energy dissipation?

Resonators terminated with long-chain alkyl groups, such as dodecyl groups, have better long-term stability than H-terminated resonators, but somewhat lower quality factors [14]. Qualitatively, an alkyl monolayer is similar to a solid alkane, such as paraffin. Since a wax resonator would presumably be highly dissipative, the low Q of the alkyl-terminated resonators was not surprising. The most surprising result,

however, emerged from experiments in which the resonators were terminated with methyl groups. The Q of the methyl-terminated resonators was better than both H-terminated and longer-alkyl-chain-terminated resonators [15]. This large discrepancy was puzzling. In chapter 3, a systematic study of the effects of alkyl-chain-length explains this effect in terms of monolayer density and packing. Simply put, the small methyl groups are able to functionalize every site on the surface, whereas the longer-alkyl-chain-terminated surfaces are limited to ~50% surface packing.

1.4 Functionalization of Resonator Surfaces – The Use of Three Different Synthetic Strategies

To serve as a chemical sensor, the surface of a micromechanical resonator must be functionalized so that it binds selectively and specifically with the analyte of interest, as illustrated by Fig. 1.2. In this cartoon, the surface is functionalized with molecules ("binders") that are specific to the rectangular analyte. All other analytes are repelled from the surface. If this is the case, any change in the effective mass of the device can be attributed specifically to the addition of rectangular analyte molecules. Thus, a change in resonant frequency can be used to determine the total mass of absorbed analyte.

For functionalization of surfaces, it is necessary to use a molecule with two functional groups – a *tether* that will anchor the moiety to the silicon surface and a *binder* that will be used for binding the analytes. In previous experiments, we successfully fabricated high-Q functionalized resonators with a Si-C tether using a Grignard-reagent-based reaction [16]. Methyl-terminated resonators had exceptionally high Q's. The challenge lay in introducing binder groups to the resonator surfaces.

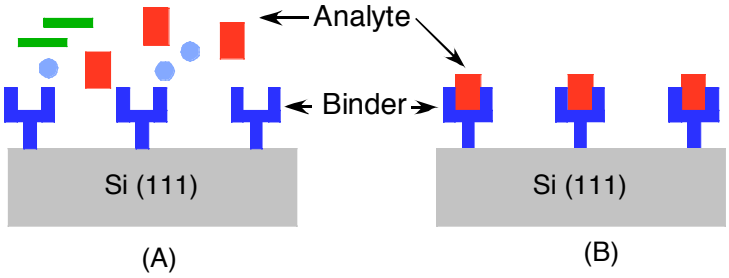

Figure 1.2 Representation of the interaction between a binder and an analyte. (A) Modified silicon surface in the presence of different analytes; (B) Interaction of the modified surface with a single analyte. This interaction is governed by the binder on the surface.

In this work, three different methods for the production of micromechanical resonators with (in principal) arbitrary surface functionalizations have been tested. All of the experiments have involved mixed monolayers containing a low density of sensor moieties distributed in a methyl monolayer. In chapter 4, organic molecules with acetal protecting groups were attached to the surface. Acetal – a common protecting group – can be transformed into a variety of functional groups using standard chemical reactions [17]. Although this approach produced resonators with high quality factors during initial processing, the harsh conditions needed for the deprotection reaction led to low Q resonators. In chapter 2, an attempt to use "click chemistry" to functionalize resonators is described. Although the successful functionalization of silicon surfaces by this approach has been reported in literature [18], we were unable to reproduce this data, in part because of the low reactivity of the mixed alkali:acetylide-acetyl Grignard reagent used in this experiment. In chapter 5 the final (successful!) strategy for surface functionalization is discussed. In this strategy, functional molecules were attached to a terminal alkene scaffold on the resonator surface using olefin cross-metathesis reaction employing Grubbs' 1st

generation catalyst [19]. As proof of principle, ester-terminated resonators with high quality factors and long-term stability were produced. The chemical strategies using in this work are summarized in Fig. 1.3.

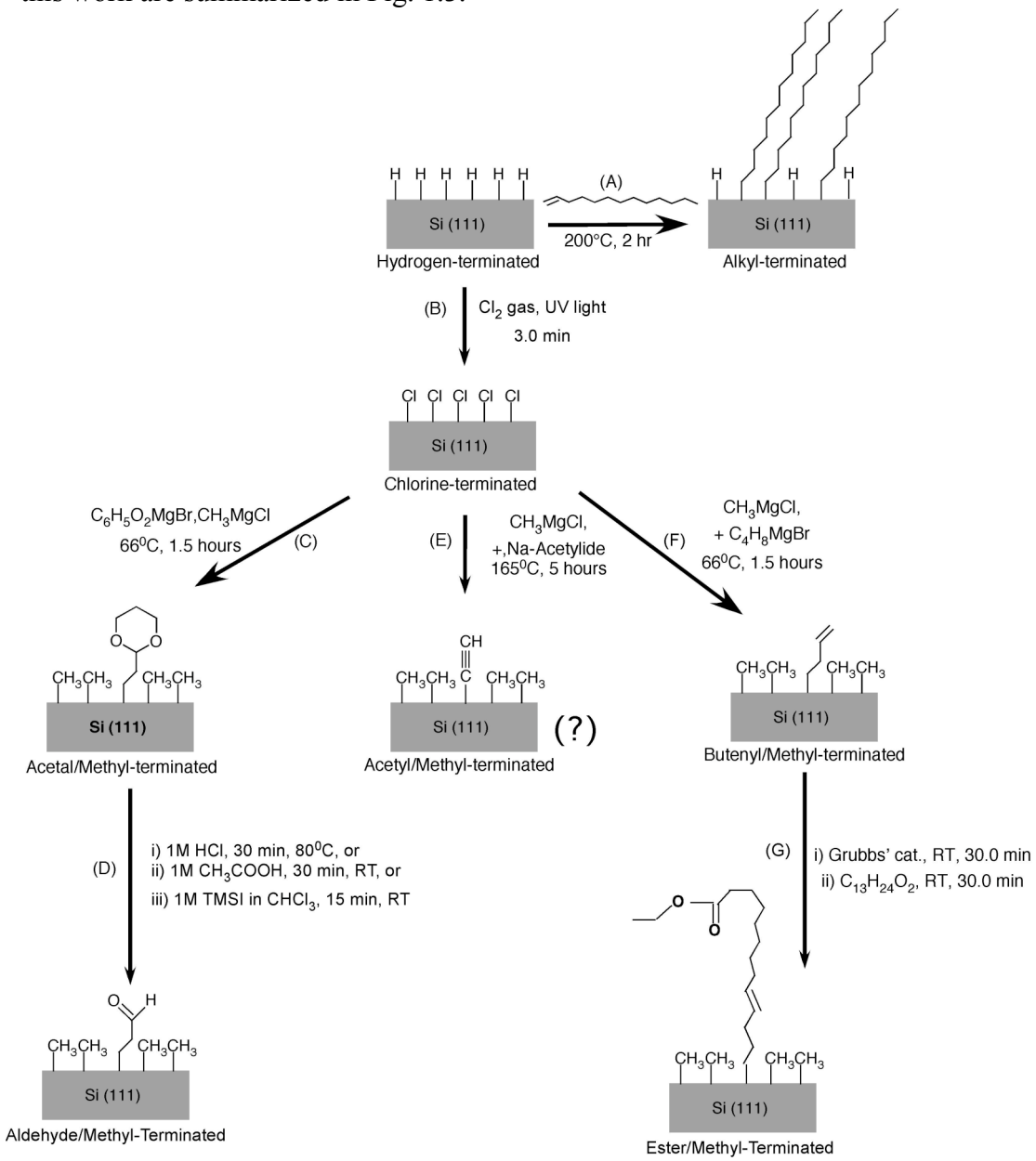

Figure 1.3 The chemical reactions used to functionalize silicon surfaces. (A) Hydrosilylation; (B) Chlorination, the first step in reactions using Grignard reagents; (C), (D) Functionalization with aldehyde using the deprotection technique; (E) Functionalization using sodium acetylide; (F), (G) Direct functionalization with ester group using olefin cross-metathesis.

REFERENCES

1. Y. Nakagawa, R. Schafer, and H.-J. Gundtherodt, *Appl. Phys. Lett.* **73**, 2296 (1998).

2. J. Chang, *IEEE Electron Device Lett.* **14**, 246 (1993).

3. U. Durig, H. R. Steinauer, and N. Blanc, *J. Appl. Phys.* **82**, 3641 (1997).

4. T. Thundat, E. A. Wachter, S. L. Sharp, and R. J. Warmack, *Appl. Phys. Lett.* **66**, 1695 (1995).

5. T. R. Albrecht, P. Grutter, D. Horne, and D. Rugar, *J. Appl. Phys*. **69**, 668 (1991).

6. K. L. Ekinci, Y. T. Yang, and M. L. Roukes, *J. Appl. Phys.* **95**, 2682 (2004).

7. F. R. Blom, S. Bowstra, M. Elwenhoek, and J. H. Fluitman, *J. Vac. Sci. Technol. B*, **10**, 19 (1992).

8. R. E. Mihailovich and N. C. MacDonald, *Sens. and Actuators* **50**, 199 (1995).

9. V. B. Braginsky, V. P. Mitranov, and V. I. Panov, *Systems with Small Dissipation* (University of Chicago Press, Chicago, 1985).

10. K. Y. Yasumura, T. D. Stowe, E. M. Chow, T. Pfafman, T. W. Kenny, B. C. Stipe, and D. Rugar, *J. Micromech. Sys.* **12**, 487 (2003).

11. J. Yang, T. Ono, and M. Esashi, *Appl. Phys. Lett*. **77**, 3860 (2000).

12. D. W. Carr, S. Evoy, L. Sekaric, J. M. Parpia, and H. G. Craighead, *Appl. Phys. Lett.* **75**, 920 (1995).

13. Y. Wang, J. A. Henry, A. T. Zehnder, and M. A. Hines, *J. Phys. Chem. B* **107**, 14270 (2003).

14. J. Henry, Y. Wang, and M. A. Hines, *Appl. Phys. Lett.* **84**, 1765 (2004).

15. Y. Wang, J. A. Henry, D. Sengupta, and M. A. Hines, *Appl. Phys. Lett.* **85**, 5736 (2004).

16. A. Bansal, X. Li, I. Lauerman, and N. S. Lewis, *J. Am. Chem. Soc.* **118**, 7225 (1996).

17. M. B. Smith, and J. March, *Advanced Organic Chemistry – Reaction Mechanisms, and Structure* (John Wiley & Sons, Inc. 2001).

18. P. T. Hurley, E. J. Nemanick, B. S. Brunschwig, and N. S. Lewis, *J. Am. Chem. Soc*. **128**, 1990 (2006).

19. L. Yang, Y.-Y. Lua, M. Tan, O. A. Scherman, R. H. Grubbs, J. N. Harb, R. C. Davis, and M. Linford, *Chem. Mater.* **19**, 1671 (2007).

Chapter 2

Experimental

2.1 Introduction

This chapter discusses the experimental techniques used in later chapters. Section 2.2 describes the fabrication of MHz-frequency silicon micromechanical oscillators. Mechanical properties of the resonators were studied using a non-invasive interferometric method, as described in section 2.3. Section 2.4 discusses the different chemical methods used to functionalize the resonators. After functionalization, the chemical state of the surfaces was characterized using Fourier transform infrared (FTIR) absorption spectroscopy and X-ray photoelectron spectroscopy (XPS), as described in section 2.5.

2.2 Resonator Fabrication

Torsional silicon resonators were fabricated at the Cornell NanoScale Science and Technology Facility (CNF) using standard fabrication techniques. Figure 2.1 (A) shows a scanning electron microscopy (SEM) image of a typical device. The micromechanical resonators consisted of hexagonal masses with supporting beams, as shown in Fig. 2.1(B). Oscillators with varying paddle widths – 4.2 μm, 5.7 μm and 7.2 μm measured across the flats – were used in the measurement of mechanical properties. The size of the supporting beams was constant for all three paddle sizes, with a length of 4 μm and a width of 440 nm. The thickness of the resonators varied between 350 nm and 425 nm and was dependant on the time of KOH etching. The thickness can be calculated from

$$t = t_0 - rT \qquad (2.1)$$

where t_0 is the thickness of the resonator before etching, r is the rate of Si(111) etching using 70°C 50% (w/v) KOH, and T is the time of etch. The etch rate has been measured to be 16.6±5.2 nm/min [1].

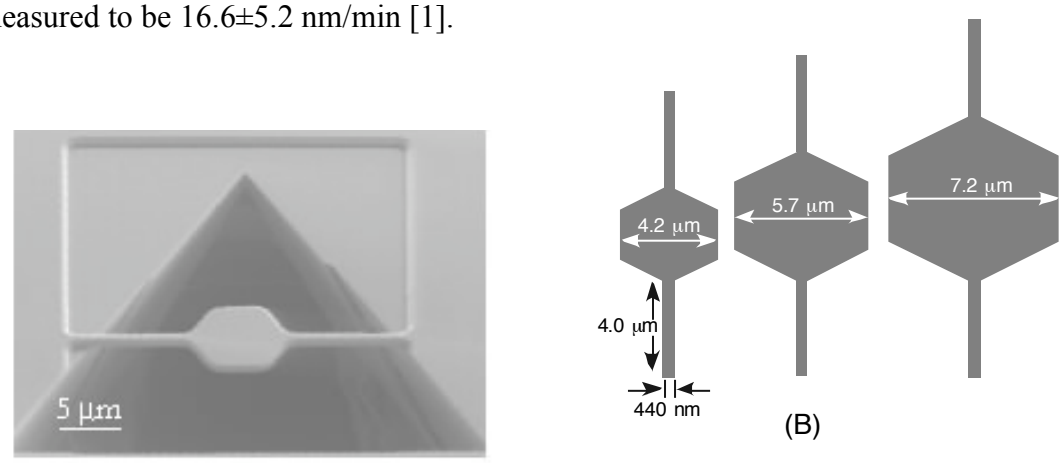

(A) **(B)**

Figure 2.1 (A) SEM image of a typical 5.7-μm-wide Si(111) resonator. (B) Cartoon showing the dimensions of the three resonator sizes. The thickness of the resonators varied between 350 nm and 425 nm.

The resonant frequencies of the devices varied from 4 MHz to 13 MHz, depending on the size of the resonator. The experimentally measured torsional frequency, f_{tors}, of the devices was previously shown by Wang *et al.* [1] to obey,

$$f_{tors} = c_{tors}\left(1.03\frac{t}{D^2}\sqrt{\frac{\beta G w}{\rho L}}\right) \quad , \qquad (2.1)$$

where D is the width of the central hexagonal mass measured across the flats, w and L are the width and length of the supporting wires, respectively, ρ is the density of silicon, β is a constant [2] that varies with w and t, and G is the shear modulus of silicon. The value of c_{tors} was calculated from finite element modeling and global fit to experiment.

The resonators were fabricated from lightly *p*-doped, float-zone silicon(111) wafers with resistivities greater than 1000 Ω-cm. In this design, {111} faces make up

approximately 77-84% of the surface area of the resonator (depending on resonator size.) Si{111} faces were chosen specifically because these faces can be etched to produce extremely homogenous, hydrogen-terminated surfaces [3] with very low surface stress [4] and ultra-low defect densities [5]. The shape of the suspended mass was chosen to be hexagonal and the etch pits triangular to take advantage of the three-fold symmetry of the {111} surface. This design prevented undercutting of the resonator supports during fabrication (*vide infra*). A combination of optical lithography, reactive ion etching (RIE) and wet chemistry was used to fabricate the resonators. Critical point drying and metallization were specifically avoided to minimize contamination.

An overview of the fabrication process is shown in Fig. 2.2. Briefly, the shape of the hexagonal paddles and supporting beams was first defined using optical lithography. The thickness of the paddles and supporting beams was then defined using reactive ion etching (RIE). A 100-nm-thick layer of thermal oxide was grown on the surface of the wafers to protect the resonator structures. A second step of optical lithography and RIE was used to define the triangular wells surrounding the resonators. The resonators were then released from the bulk by etching in a highly anisotropic etchant – 40% w/v (aq) KOH at 72.2°C for 5 min. The protective oxide layer was then removed with a 5:1 solution of room temperature NH_4F(aq):HF(aq), known as buffered oxide etchant (BOE, Transene), for 90 sec. In the following sections, each processing step is discussed in detail.

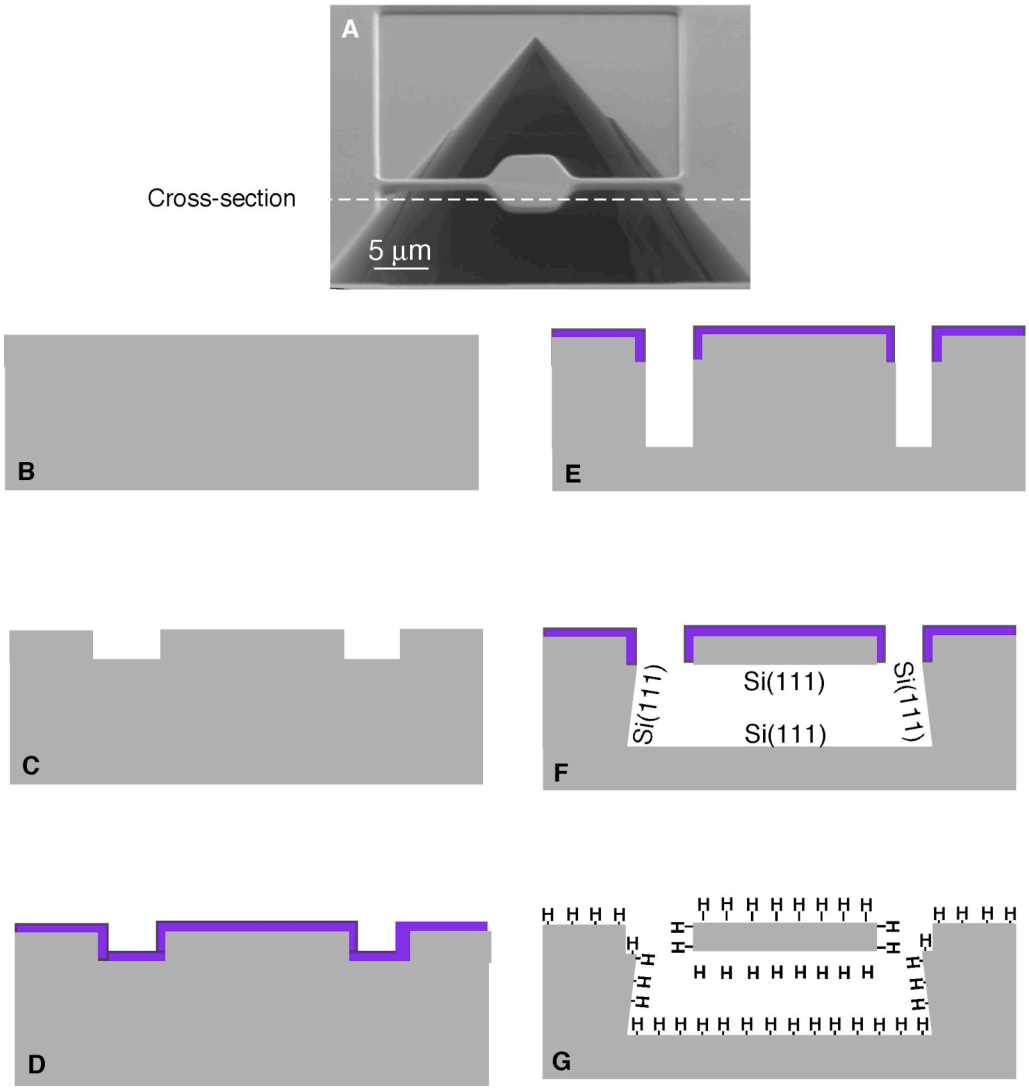

Figure 2.2 Schematic of the fabrication process (not to scale). (A) SEM image of a 5.7-µm-wide resonator, indicating the cross-section (white dashed line) that is sketched in (B)-(G); (B) Initial Si(111) wafer, shown in gray; (C) First lithography step followed by RIE defined the shape and thickness of the resonators; (D) The surface was protected with 100 nm of thermal oxide, shown in purple; (E) Second lithography step followed by RIE defined deep trenches in the silicon wafer; (F) Hot KOH was used to etch non-{111} faces; (G) Protective oxide was removed using buffered oxide etchant (5:1 NH_4F(aq):HF(aq))

2.2 (i) Optical Lithography

Before fabrication, the silicon wafers were immersed in BOE for 30 sec to remove any native oxide, rinsed in ultrapure water, and dried with a stream of N_2. The wafers were loaded into a YES LP-III oven and coated with a layer of hexamethyldisilazane (HMDS) to promote photoresist adhesion. The wafers were placed on a circular chuck and vacuum clamped. OiR 620-7i *i*-line photoresist was pipetted onto the center of the wafer, and the wafer rotated at 4000 rpm for 60 sec. Care was taken to ensure that the wafer was coated with a uniform layer of photoresist at the end of the spin cycle. This procedure yielded a uniform 0.55-μm-thick photoresist layer. The wafer was then transferred to a hotplate and heated for 60 sec at 90°C. This process, known as a "soft bake," removed any residual solvent and hardened the photoresist.

Chrome masks for the first and second stages of photolithography were designed on the GCA/MANN 3600F optical pattern generator. The 10× *i*-line stepper was used to transfer the design onto the photoresist-coated wafers. The stepper reduces the design on the chrome mask by a factor of ten and has a minimum feature size of ~ 0.6 μm. The resonator pattern was printed in a 12×12 array of dies on a 500-μm-thick, 100 mm diameter wafer. The spacing between adjacent dies was 0.25″. After exposure to UV light in the stepper, the wafer was returned to a hotplate for a "hard" or post-exposure bake. For the OiR 620-7i resist, this involved heating at 115°C for 60 sec to improve the resist contrast. The wafer was then developed in a Hematech Steag wafer processor. Alternating spray– and puddle–processing was used with AZ300 MIF wafer developer at room temperature for 90 sec. The AZ300 MIF solution dissolved the non-UV-exposed regions of the photoresist on the wafer, removing the regions that had been exposed to UV light. The remaining resist was then used as a

mask in the following RIE process. The wafer was then rinsed in ultrapure water and dried using N_2.

The optimum time of exposure to UV light and the focus of the 10× *i*-line stepper was determined by first varying exposure times and foci on a test wafer. After developing the resist on the test wafer, the dies were studied with an optical microscope. The parameters of the die with the sharpest focus and best exposure were used for all other wafers.

2.2 (ii) Reactive Ion Etching

The thickness of the resonators was defined by reactive ion etching using the PlasmaTherm SLR 770 (PT 770) as shown in Fig 2.2 (B). After lithography, the patterned photoresist was used as a mask for the RIE process. Before loading the wafer into the PT 770, a *Q*-tip™ was soaked in acetone and a thin bead of photoresist removed from the edge of the wafer to prevent the wafer from sticking to the wafer clamp inside the machine. A dry chlorine etch at ~4°C was performed for 1.5 min. During this process, a mixture of chlorine-containing gases removed 300-450 nm of exposed silicon. This process was followed by a thorough rinse in ultrapure water and drying under N_2. The wafers were then vacuum clamped onto spinner chucks and sequentially sprayed with acetone and isopropyl alcohol and rotated at 4000 rpm. The acetone and isopropyl alcohol rinsing procedure was repeated twice to ensure complete resist removal.

2.2 (iii) Thermal Oxidation

After the shape and thickness of the resonators was defined, a layer of thermal oxide was grown on the wafers, as shown in Figure 2.2 (C). The oxide layer served as a protective coating, preventing resonators from being etched away during the KOH etch process.

Prior to oxidation of the surface, the wafers were cleaned using the standard RCA clean [3] as follows. The wafers were immersed in a 6:1:1 solution of $H_2O(l):H_2O_2(aq):NH_4OH(aq)$ at 70°C for 10 min, then rinsed in 16 MΩ-cm water. The wafers were then immersed in a 6:1:1 solution of $H_2O(l):H_2O_2(aq):HCl(aq)$ at 70°C for 10 min and again rinsed in 16 MΩ-cm water. The wafers were then immersed in concentrated HF for 15 sec to remove the oxide, rinsed in 16 MΩ-cm water and spin-dried.

Two methods of oxide growth were available at the CNF – a wet oxide and a dry oxide process. The dry oxide process results in a more uniform, pinhole-free oxide and was always used in processing. The RCA-cleaned wafers were loaded into the oxide furnace at a temperature of 900°C. The temperature was then slowly ramped to 1050°C. The wafers were oxidized in pure $O_2(g)$ at this temperature for 55 minutes followed by annealing for a further 30 min in $N_2(g)$. The temperature of the furnace was then ramped down to 900°C, and the wafers removed. The annealing process results in a smooth Si/SiO_2 interface [4]. The thickness of the oxide layer was approximately 100nm. The resulting wafer appeared dark blue because of interference in the SiO_2 layer [5].

2.2 (iv) Second Photolithography and RIE Processes

Before release of the resonator from bulk silicon, a second lithography process was required to define the deep trenches around the resonators. For the second lithography step, the wafers were coated with SPR220 3.0 (Shipley) photoresist – a thicker resist than the OiR 620-7i resist used in the first photolithography step. The structural dimensions on the second mask were bigger than those of the first lithography process and required less stringent focus and exposure control. Because of this, a thicker resist could be used. The wafers were first vapor primed in the YES oven as discussed in Sect. 2.2 (i) and then vacuum clamped to a spinner. Resist was applied to the center of the wafer. The wafers were then spun at 5000 rpm for 60 sec, resulting in a 2-μm-thick layer of resist. The wafers were visually checked for resist uniformity and the process repeated as necessary. A "soft bake" was performed at 130°C for 90 sec.

Precise alignment between the first and second layers of photolithography was essential to prevent damage to the resonators during the KOH release process. The fiducial marks defined on the wafer during the first lithography process were used for alignment as shown in figure 2.3 (A). The correct offset in *x*- and *y*-directions were calculated by exposing a test wafer, measuring the misalignment between the two layers and then correcting. The optimum offset was then applied to all wafers. Figure 2.4 (B) shows the correct alignment of the resonators defined on the two layers.

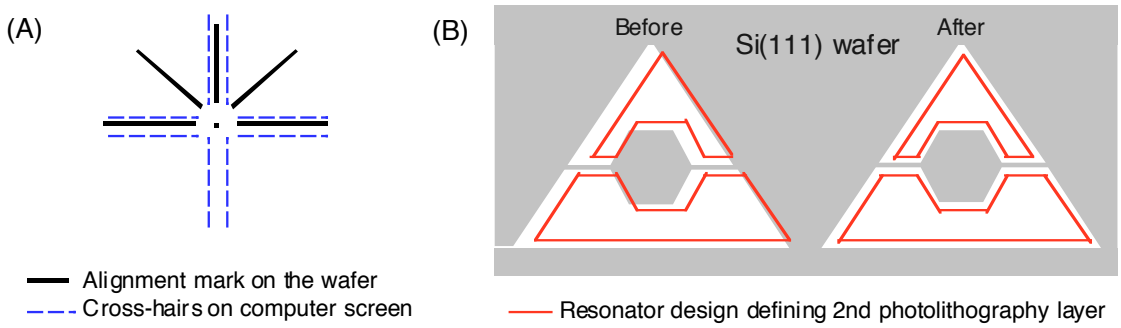

Figure 2.3 Schematic representation of the alignment process used on the 10× *i*-line stepper. (A) Alignment of second layer based on the alignment marks defined on the wafer during the first photolithography step; (B) The resonator design of the two layers before and after alignment. See text for more detail.

After exposure in the 10× *i*-line stepper, the wafers were "hard baked" at 130°C for 60 sec. This was followed by development of the pattern in the Hematech Steag wafer processor using AZ300 MIF solution. The developed resist was used as a mask for following RIE processes.

The PlasmaTherm 72 RIE system (PT 72) was used to etch the trenches and the resonators. To remove any contamination in the chamber from previous use, an O_2 clean (process #0) was first performed on an empty chamber for 2 min. The wafers were placed in the PT 72 chamber, and a fluorine-based RIE process (25:1 CHF_3:O_2, process #1) was performed for 8 minutes. During this process, unprotected SiO_2 was selectively etched, resulting in the removal of all unmasked oxide and exposure of the underlying silicon. The wafers were then moved into the Unaxis SLR 770 ICP Deep Silicon Etcher (Unaxis 770). In the Unaxis 770, the Bosch process, a fluorine-based etching process using SF_6, was used to etch deep trenches around the resonators. Each SF_6-etching step was alternated with a C_4F_8-deposition step that strengthened the side-walls and passivated them towards chemical attack. The wafers were exposed to

approximately 50 cycles, resulting in the formation of 10-μm-deep triangular trenches around the resonators.

After fabrication, the wafers were diced into 0.25″×0.25″ squares using a K&S wafer saw with a thin diamond blade. Each wafer generated 144 identical samples, each containing four arrays of 21 resonators at the sample center. Figure 2.4 shows the arrangement of the resonators on each sample. The central red resonator is oriented at 0° to the parallel axis of the resonator. The orientation of the other resonators varied with respect to the central resonator, with the resonators to the right oriented at 1°, 2° and 3° to the Si(111) plane and the resonators to the left oriented at -1°, -2° and -3°. Mechanical property measurements showed that resonator quality was independent of these small changes in orientation. For consistency, the central resonator, denoted in red, was used for all further measurements. Spatial variations in processing (*e.g.,* RIE etch rate) led to small variations in resonator thickness and thus frequency. To enable the direct comparison of resonators with nearly identical mechanical properties, the samples were numbered before dicing to facilitate later identification of adjacent samples.

2.2 (v) Final Release of Resonators

After fabrication, residual resist was removed from the silicon samples with an overnight soak in acetone. Before each experiment, a modified RCA clean [6] was used to remove all surface contaminants from the sample chip. The chip was first immersed in a solution of 4:1:1 H_2O(l):H_2O_2(aq):NH_4OH(aq) at 80°C for 10 minutes (SC1), followed by thorough rinsing in 18.2 MΩ-cm water (Millipore Milli-Q). The sample was then immersed in a solution of 4:1:1 H_2O(l):H_2O_2(aq):HCl(aq) at 80°C

for 10 minutes (SC2) followed by rinsing with ultrapure water. A second 10 min SC1 clean and subsequent rinsing with ultrapure water completed the cleaning process.

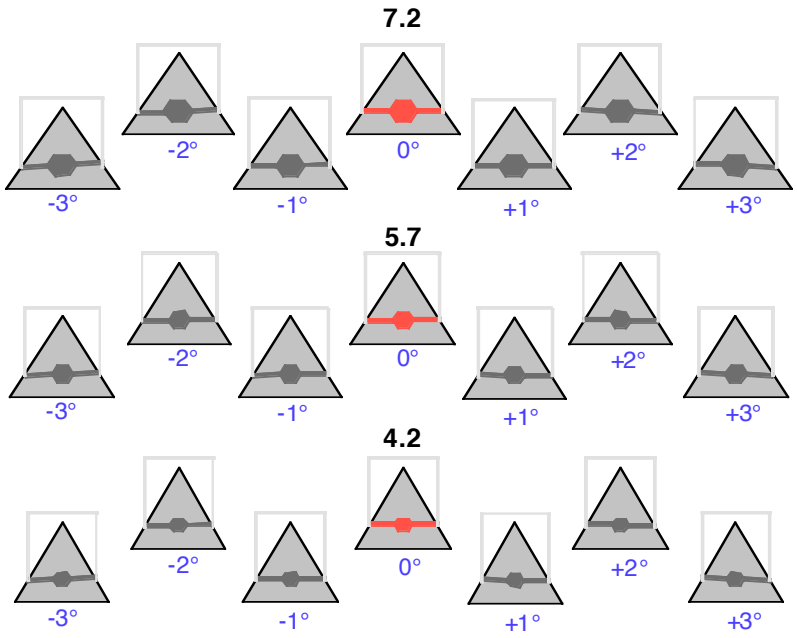

Figure 2.4 Arrangement of resonators on a single 0.25″×0.25″ silicon sample. Each sample contains four identical arrays of resonators, one of which is shown above. The resonator used in mechanical property measurements is shown in red.

Once cleaned, the resonators were released from the bulk using the anisotropic etching properties of potassium hydroxide (KOH) as illustrated in Fig 2.2 (E). Aqueous KOH is an anisotropic etchant that selectively etches non-{111} silicon planes without etching SiO_2 [7]. The SiO_2 thus acts as an etch mask during this process. The cleaned samples were immersed in 72.2°C KOH (50% w/v, LabChem) for 5 min, then rinsed thoroughly in ultrapure water. The sample was etched in BOE for 1.5 min at room temperature followed by rinsing in ultrapure water. The resulting surface of the sample was hydrogen-terminated, as shown in Fig. 2.2 (F).

2.3 Mechanical Property Measurements

2.3 (i) Optical Interferometry

Resonator motion was detected with the optical interferometer shown in Fig 2.5. The output of a 633 nm, 8 mW He-Ne laser was adjusted using a linear polarizer, passed through a 100 mm focal length lens and transmitted through a polarizing beam splitter. A quarter-wave plate converted the linearly polarized light into circular polarized light, which was then focused onto the hexagonal paddle of the resonators using a 10× objective lens. The resonators behaved as Fabry-Perot interferometers. The incident light was reflected from both the surface of the resonator as well as the underlying bulk (after transmission through the resonator), as shown in Fig 2.6. Motion of the resonator resulted in a change in the intensity of the interferometric signal. The reflected light passed through the quarter-wave plate once again and was converted back to linearly polarized light and transmitted through the beam splitter to a photodetector (DET210, Thorlabs). The output of the photodetector was sent to a spectrum analyzer to be analyzed.

To prevent mechanical energy dissipation due to viscous drag losses, the resonators were operated at 10^{-8} Torr in an ion-pumped vacuum chamber. After loading the samples, the chamber was first evacuated to approximately 10^{-3} Torr using a liquid-N_2-cooled sorption pump containing molecular sieves. A 25 L/s Perkin-Elmer ion pump was then started, and the chamber evacuated to a pressure of 10^{-8} Torr. A pneumatic gate valve was used to isolate the ion pump from the chamber during loading and unloading of the sample. To aid alignment, a white light source was directed coaxially with the laser beam and used to illuminate the resonators. The reflected image was focused on a CCD camera and displayed on a monitor. The

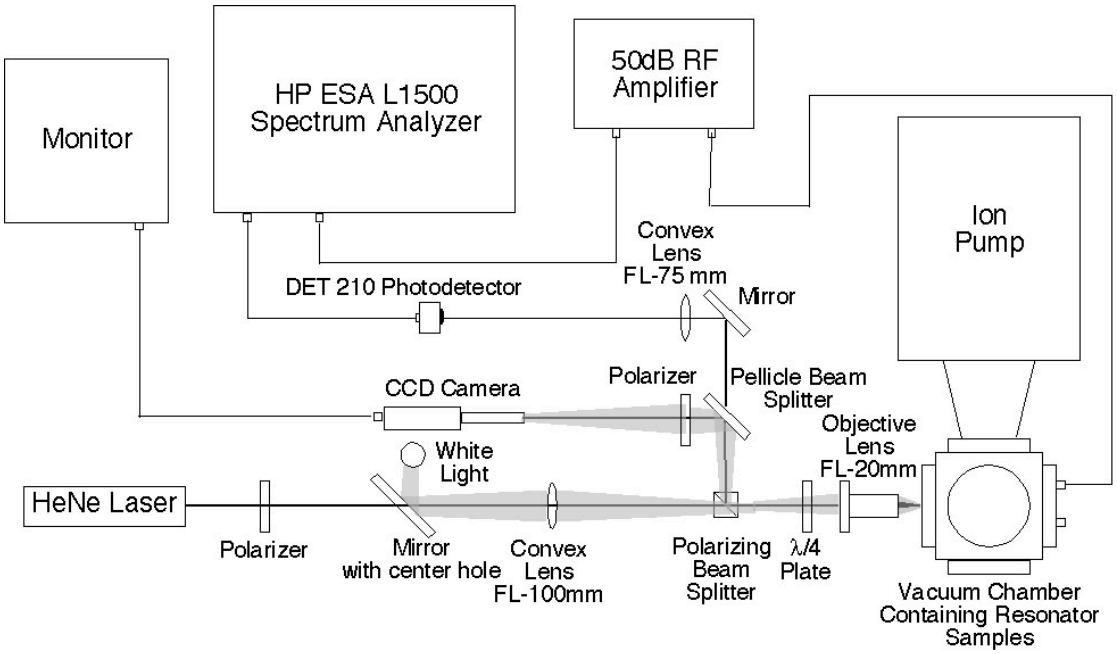

Figure 2.5 Schematic of the optical interferometer used to measure the mechanical properties of resonators.

resulting image was used to precisely position the laser beam on the hexagonal paddle of the resonator. The position of the laser on the sample was controlled by a 3-axis translational stage that supported the vacuum chamber. To prevent external vibrations from disturbing the optical interferometer, the entire interferometer was mounted on a vibration-isolated optical table.

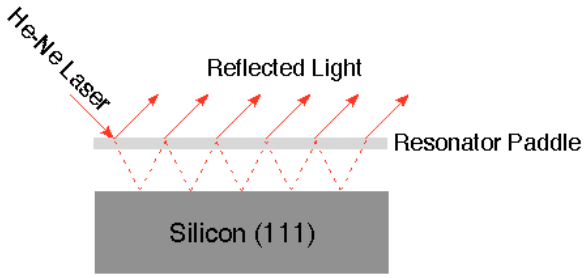

Figure 2.6 Schematic of Fabry-Perot interferometer formed by oscillating paddle and stationary substrate.

2.3 (ii) Piezo-Actuated Drive

The resonator samples were clamped to a lead zirconate titanate (PZT) ceramic disk (7/16″ thick, 0.75″ diameter, resonant frequency of 200 kHz, Stavely), as shown in Fig 2.7. Copper wires were soldered onto the 0.0005″ Ag electrodes on the top and bottom of the PZT disk using UHV-compatible Sn-Ag alloy and connected to BNC feedthroughs. An AC voltage of approximately 12.0V, generated by a Hewlett-Packard spectrum analyzer (ESA L1500), was amplified using a 50 dB RF amplifier (EIN Model 325LA, 250 kHz-150 MHz), which was connected to the bottom electrode of the PZT disk. The top piezo electrode was grounded. When an AC voltage was applied to the piezoceramic disk, the disk expanded and contracted along the direction of polarization, resulting in resonator motion.

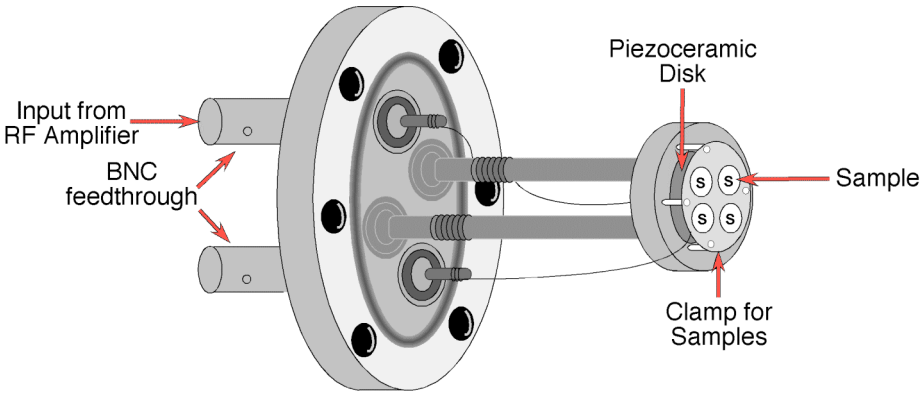

Figure 2.7 Schematic of the sample holder used to load up to four 0.25″×0.25″ samples into the vacuum chamber.

2.3 (iii) Mechanical Property Measurements

The interferometric signal was analyzed with the spectrum analyzer and the data communicated to a computer using a General Purpose Interface Bus (GPIB,

National Instruments) interface. A typical Fourier transform of the interferometric signal is shown in Fig 2.8. The resonant frequencies of oscillation were determined by first measuring resonant response over a wide frequency range (*e.g.* 4 MHz to 17 MHz). The resulting signal was fit to a Lorentzian lineshape in order to determine the resonant frequency (*i.e.* peak position) and the full-width-half-maximum, Δf. The fit was done using IgorPro v. 5.0, which uses a least squares method to formulate a Lorentzian curve to fit the given data, generate co-efficients of the Lorentzian curve and their associated errors. For the experiments described in this dissertation, the error observed for Q varied from ±100 up to ±1000. The residual shown in Fig. 2.8 indicates how closely the Lorentzian curve fits the experimental data. In Fig. 2.8, the residual is mainly noise, signifying that the curve fits the data very closely.

The quality factor, Q, of the resonator was determined from

$$Q = \frac{1.54 f}{\Delta f} \qquad (2.2)$$

Translational vibrational modes were distinguished from torsional modes using the characteristic shape of the response. Translational modes have a distorted (non-Lorentzian) lineshapes at high drive amplitudes, because these modes are more susceptible to non-linearities [8, 9].

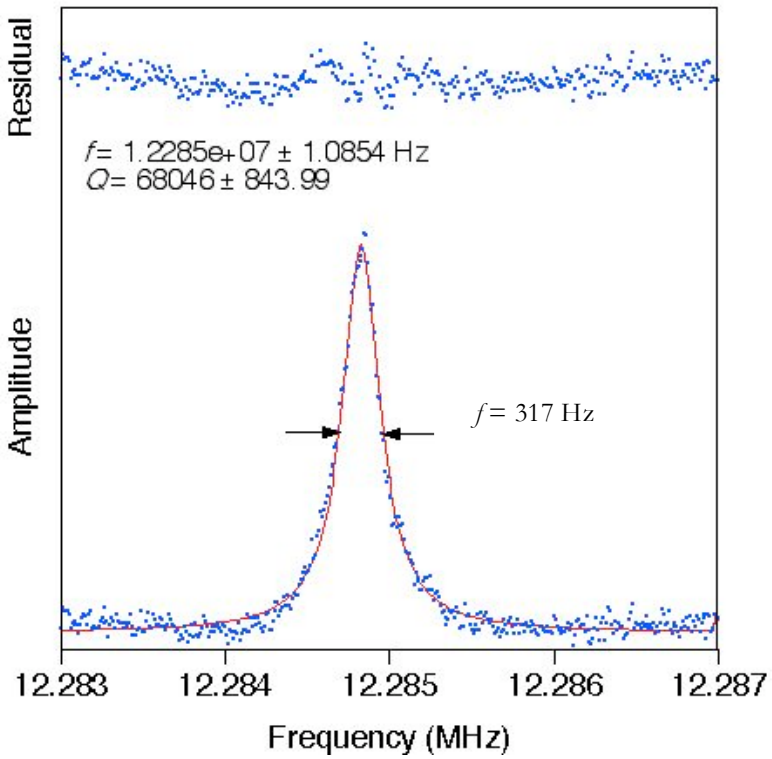

Figure 2.8 Representative data from mechanical property measurements. Data was fit to a Lorentzian curve (red trace) to determine *f* and *Q*.

2.4 Chemical Modification of Surfaces

Although methyl-terminated resonators have very high *Q* [10], these waxy coatings also inhibit surface adsorption. For sensing purposes, reactive functional species must be attached to the resonator surface. Most functional groups, however, are larger than methyl groups, and this introduces a serious problem. Previous results have shown that the high qualities of methyl-terminated resonators are the result of their ability to terminate every site on the surface. Functional groups that are even slightly larger than methyl groups (e.g., ethyl groups) terminate at most 50% of surface sites. To produce fully functionalized, high-*Q* resonators with chemical specificity, we chose a strategy based on mixed monolayers. In this strategy, most

surface sites are terminated by methyl groups; however, a low density of chemically active sites were also included in the monolayer. In this work, three different strategies for functionalization were used for the production of mixed monolayers.

In the first strategy, an acetal/methyl-terminated surface was prepared. The usefulness of acetal chemistry as a functionalization tool lies in the ease of conversion of the acetal into a variety of different functional groups. For example, simple chemical reactions can be used to convert acetals into alcohols, aldehydes, carboxylic acids or amines [11]. In the second strategy, an attempt was made to use so-called "click" chemistry [12] to attach organic functionality. In "click" chemistry, two reactive molecules selectively "click" together via a covalent bond. The aim of this strategy was to terminate surfaces with acetyl molecules to enable the azide-alkyne Huisgen cycloaddition. The first two strategies were deemed unsuccessful for universal functionalization applications for the following reasons. First, the termination of resonators with mixed-methyl-acetal monolayers resulted in high Q, but the subsequent transformation of the acetal to an aldehyde dramatically decreased resonator quality. This decrease in Q was attributed to the harsh reaction conditions. Second, the termination of resonator with sodium acetylide did not go to completion, probably as a result of the low reactivity of the reagent. Third, exposure of the surfaces to organic solvents at elevated temperatures – which is required for both strategies – had a deleterious effect on resonator quality factor.

The final strategy therefore used mild reaction conditions for surface functionalization. In this method, surface functionalization was introduced using an olefin metathesis reaction between terminal olefins on the resonator surface and a terminal olefin on an organic molecule. The reaction was catalyzed by the Grubbs' catalyst. This catalyst reacts with terminal alkene bonds with high selectivity and is

inert towards most other functionalities. In principle, this strategy can be used for the attachment of almost any desired functionality.

The experimental details of the different surface termination chemistries are discussed in detail in the following sections.

2.4 (i) Formation of Alkyl Monolayers Using Hydrosilylation

H-terminated silicon resonators were reacted with either 1-dodecene ($C_{12}H_{25}$, >95%, Aldrich) or 1-octadecene ($C_{18}H_{37}$, >95%, Aldrich) as follows. The reagent was first purified by drying over molecular sieves for at least 24 hours followed by distillation under vacuum. The distillate was collected in a Strauss flask, a round-bottom flask with a sealable sidearm, under inert conditions and transferred to an oxygen– and water–free glove box which was continuously purged with N_2. Hydrogen-terminated samples, the preparation of which has been described in Sect. 2.2 (v), were placed in a glass vial, sealed with a Teflon cap and transferred to the glove box. Inside the glove box, enough alkene was added to the glass vial to completely cover the sample and the vial re-sealed. The sealed glass vial was removed from the glove box and placed in a mineral oil bath pre-heated to 200°C. The sample was heated in the alkene for 1 hour, after which the vial was allowed to cool, and the sample was thoroughly rinsed in methylene chloride. The resulting surface was hydrophobic. The hydrophobicity of the surface was tested using a drop of water.

2.4 (ii) Formation of Alkyl Monolayers Using Grignard Reagents

A two-step process [13] was used to synthesize alkyl-terminated resonators from Grignard reagents. In the first step, a hydrogen-terminated sample, which was

prepared using the procedures described in Sect. 2.2 (v), was placed in a quartz round-bottom flask, fitted with a condenser and attached to a Schlenk line. The flask was thoroughly purged with argon and then evacuated to approximately 40 mTorr as measured on a MKS convection gauge. Chlorine gas was introduced into the line at approximately 50 Torr as measured using a Monel Matheson 63-5601M gauge. The flask was irradiated with a Hg pen lamp for 3.0 min. This process converted the hydrogen-terminated surface to a chlorine-terminated surface [14]. The chlorine gas was evacuated and the flask filled with argon.

In the second step, enough alkylmagnesium halide (CH_3MgCl, 3.0 M in THF, Sure-Seal, Aldrich; C_2H_5MgBr, 0.5 M in THF, Sure-Seal, Aldrich; $C_{12}H_{25}MgBr$, 0.5 M in diethyl ether, Sure-Seal, Aldrich; $C_{18}H_{37}MgCl$, 0.5 M in THF, Sure-Seal, Aldrich) was transferred into the round–bottom flask using a double-tipped cannula under a positive pressure of argon to completely cover the sample. The sample was refluxed in the reagent for 1.5 hr (methyl), 2.5 hr (ethyl), or 40 hr (dodecyl and octadecyl) under continuous Ar purge. At the end of the reaction, the cooled reagent was diluted with tetrahydrofuran (THF, Aldrich, > 95% purity) in ambient air and then decanted. Unreacted reagent was neutralized using anhydrous methanol. The functionalized sample was finally rinsed successively in methylene chloride and water. The resulting surface was hydrophobic, and tested with a water droplet.

2.4 (iii) Formation of 1,3-Dioxan-2-ylethyl / Methyl Mixed Monolayers

Our first strategy for the introduction of reactive functional groups used an acetal/methyl mixed monolayer – a small number of acetal moeites dispersed within a predominantly methyl-terminated surface. The acetal groups were then converted to an aldehyde. In the first step, Cl-terminated surfaces prepared using the strategy

described in section 2.4(ii) were immersed in reaction mixtures consisting of 1,3-dioxan-2-ylethyl Grignard reagent (acetal Grignard reagent, $C_6H_{11}O_2MgBr$, 0.5 M in THF, Sure-Seal, Aldrich) and methyl Grignard reagent [1:10, 1:2, 1:16, 1:125 (by volume)] under a constant flow of argon. [The different Grignard reagents used in these experiments vary in concentration and hence, a ratio of the volume of the constituent reagents is used as an indicator of the amount of each reagent present in the reaction mixture.] The Cl-terminated samples were refluxed for 1.5 hours (~66°C) in the mixed Grignard reagents. After the reaction, the reagent was cooled and diluted with THF under ambient air. The samples were then rinsed in anhydrous methanol, methylene chloride and ultrapure water.

Three different methods for the conversion of acetal to aldehyde were tried. In the first method, acetal/methyl-terminated surface was heated to 80°C in a 1 M HCl solution for 30 min [15] and then rinsed with ultrapure water. In the second method the functionalized surface was immersed in 1.0 M acetic acid for 30 min at room temperature [15] followed by thorough rinsing in ultrapure water. Finally, a non-aqueous method was used whereby the functionalized surface was reacted with 1.0 M solution of iodotrimethylsilane (TMSI, $(CH_3)_3SiI$, Aldrich) in chloroform for 15 minutes at room temperature [16] followed by thorough rinsing in methylene chloride and ultrapure water.

2.4 (iv) Formation of Acetyl/Methyl Mixed Monolayers

In the second functionalization strategy, a small number of acetyl moieties were introduced onto a predominantly methyl-terminated surface via a mixed monolayer in order to enable “click” chemistry [12].

A 0.5 M solution of sodium acetylide, Na–C≡C–H, (18 wt% slurry in xylenes/light mineral oil, 95%, Aldrich) in diglyme was prepared under inert conditions. A 1:1 mixture (by volume) of Na–C≡C–H in diglyme and methyl Grignard reagent was cannulated into a reaction vessel containing a Cl-terminated silicon sample under a positive pressure of Ar. The chlorination of H-terminated samples has been described in Sect. 2.4(ii). The Cl-terminated samples were immersed in the reaction mixture for 5 hours under reflux conditions (~162°C) in an inert atmosphere. After cooling, the resonator samples were rinsed with xylenes (previously dried over sodium), THF, anhydrous methanol and methylene chloride.

Two other precursors to allyl/acetyl chemistry were also tried − allyl Grignard reagent (C_3H_5MgBr, 1.0 M in diethylether, Sure-Seal, Aldrich), and ethenyl Grignard reagent (C_2HMgBr, 0.5 M in THF, Sure-Seal, Aldrich). For experiments involving the allyl and ethenyl Grignard reagents, a 1:1 mixture (by volume) of the allyl/ethenyl Grignard reagent and methyl Grignard reagent was cannulated into a reaction vessel containing a Cl-terminated silicon sample under a positive pressure of Ar. The chlorination of H-terminated samples has been described in Sect. 2.4 (ii). The Cl-terminated samples were immersed in the reaction mixture for 5 hours under reflux conditions (~67°C for allyl and ~162°C for ethenyl Grignard reagents) in an inert atmosphere. After cooling, the resonator samples were rinsed with THF/diethyl ether, anhydrous methanol and methylene chloride.

2.4 (v) Formation of Ethyl 10-Tridecenoate / Methyl Mixed Monolayers

In our final synthetic approach, we tried to find the mildest functionalization conditions possible. Since previous experiments had suggested that common organic solvents degraded funtionalized resonators, we also tried to minimize solvent

exposure– particularly at elevated temperatures. Olefin cross-metathesis reactions catalyzed by the Grubbs' catalyst was chosen for our investigations for two reasons. First, these reactions are extremely flexible – essentially any functional group can be attached in this fashion. Second, these reactions are both highly specific towards the terminal alkene and proceed under mild conditions. During our investigations, Yang et al. [17] reported a procedure for the functionalization of silicon surfaces, which we adapted.

This functionalization strategy required a surface with a low density of terminal olefins for cross-metathesis. The remaining surface sites were methyl-terminated for high *Q*. The first step in the functionalization process required the synthesis of butenyl/methyl mixed monolayers. Cl-terminated samples were prepared by Cl_2-etching of H-terminated surfaces, as described in Sect. 2.4 (ii). The Cl-terminated surface was then immersed in a 1:4 mixture (by volume) of butenyl Grignard reagent (C_4H_7MgBr, 0.5 M in THF, Sure-Seal, Aldrich) and methyl Grignard reagent (CH_3MgBr, 3.0 M in THF, Sure-Seal, Aldrich). The sample was refluxed in the reaction mixture for 1.5 hours (~ 66°C) under constant flow of argon. After cooling, the reaction mixture was diluted with THF in ambient air, then rinsed in THF, anhydrous methanol, methylene chloride and ultrapure water successively.

After forming the butenyl/methyl monolayer, the terminal olefins were selectively reacted with the Grubbs' catalyst. A 13 mM solution of 1st generation Grubbs' catalyst ($C_{43}H_{72}Cl_2P_2Ru$, Aldrich, Fig. 2.9) in chloroform was prepared under inert atmosphere. The butenylated samples were immersed in the catalyst solution for 30 min at room temperature under inert atmosphere, then rinsed thoroughly in excess methylene chloride and ultrapure water.

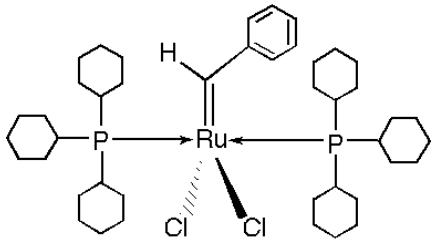

Figure 2.9. Chemical structure of the 1st generation Grubbs' catalyst

The ruthenylated sample was then transferred to a clean round–bottom flask in ambient air. Enough neat ethyl 10-undecenoate ($C_{13}H_{24}O_2$, > 97%, Aldrich) was added to the flask to cover the sample completely. The flask was then attached to the Schlenk line, degassed under vacuum, and left to react for 30 min under inert atmosphere. After reaction, the sample was thoroughly rinsed with methylene chloride and ultrapure water. At the end of the reaction, the surface was terminated with a mixture of methyl and ethyl 10-tridecenoate moieties, as shown by infrared absorption spectroscopy.

2.5 Surface Characterization Techniques

2.5 (i) Infrared Spectroscopy

Fourier transform infrared (FTIR) absorption spectroscopy was used to characterize functionalized surfaces. Spectroscopic data were collected in either the transmission or the multiple internal reflection (MIR) geometry, depending on the spectroscopic region of interest. Due to multiple reflections within the silicon sample, the MIR geometry is more sensitive to chemical species at the surface than transmission; however, multiphonon absorption in bulk silicon prohibits measurement

below 1500 cm^{-1} in this geometry. Although the transmission geometry is much less sensitive, this geometry is useful for the detection of low energy modes (450-1500 cm^{-1}).

In the MIR geometry, infrared radiation is focused onto a 1.54″×0.59″×0.02″ trapezoidal sample, as sketched in Fig 2.10 (A). After entering the sample, the radiation is internally reflected ~76 times before exiting the opposite bevel. When IR radiation is reflected from the surface of the sample, IR-active vibrational modes of surface adsorbates interact with the evanescent electric field producing a characteristic absorption spectrum.

Infrared analysis of functionalized resonators was not attempted. Instead, special samples were co-processed with the resonators, then examined spectroscopically. Infrared absorption in the transmission geometry can be performed on any double-polished silicon sample greater than 0.5″ × 0.75″ in size. In contrast, the MIR geometry requires the fabrication of special beveled samples.

To fabricate MIR samples, 500-μm-thick Si(111) wafers from the same batch as used for resonator fabrication were cut into 1.56″ × 0.59″ samples using the K&S wafer saw at CNF. The samples were glued to a special stainless steel polishing chuck using CrystalBond. The chuck holds the samples at a precise 45° angle. Initially, the sample was glued so that ~1 mm extended below the chuck. A thick layer of glue was also applied to the surface of the sample, to prevent surface damage during polishing. The protruding edge of the silicon sample was polished down to the edge of the holder using a Metaserv Grinder-Polisher (Buehler). The course polish used 620 grit silicon carbide paper at 500 rpm for 5 min, followed by 300 grit paper at 500 rpm for 5 min. This was followed by fine chemo-mechanical polishing using a slurry of 15% (w/v) KOH, isopropyl alcohol and 0.05 μm alumina. The slurry was added to the center of a

nylon polishing pad (Buehler) and the samples polished at 300 rpm until a mirror finish was observed at the beveled edge. The sample holder was then rinsed thoroughly under running water to remove any slurry. The sample was then reversed, and the opposite side polished. Once both edges were polished, the sample was removed from the polishing chuck and soaked in acetone overnight to remove any residual glue.

After surface functionalization, the sample was placed in a custom-machined Teflon sample holder, which allowed the simultaneous loading of two MIR samples. The sample holder was placed in the dry-air-purged chamber of an FTIR spectrometer (Nicolet-Nexus 670), and data collected using a liquid–nitrogen–cooled mercury cadmium–telluride (MCT-A) detector.

Infrared spectra in the transmission geometry was collected by placing the silicon sample in the IR chamber at 73° to the surface normal, as shown in Fig 2.10 (B). The sample is oriented at 73° to the surface normal in accordance with Brewster's angle measurements. The Brewster's angle for Si is calculated using the following equation where η_2 is the refractive index of silicon and η_1 is the refractive index of air, i.e., $\eta_1=1$,

$$\theta = \arctan(\frac{\eta_2}{\eta_1}), \qquad (2.3)$$

and η_2 depends on temperature and wavelength at which the refractive index is measured.

Data were collected with a deuterated–triglycine–sulfate (DTGS) detector. Depending on the organic modification of the silicon surface, either or both methods were used for surface characterization.

2.5 (ii) X-Ray Photoelectron Spectroscopy

X-Ray photoelectron spectroscopy (XPS) uses the binding energy of core electrons to characterize the chemical state of surfaces. Fig 2.11(A) illustrates the XPS process. Incident x-rays penetrate the sample to a depth of ~1 μm, exciting many core electrons in their path. Almost all of the excited electrons lose their kinetic energy via interactions with bulk atoms. Only those electrons excited in the top 5-10 nm of the sample retain enough energy to exit the sample. These electrons are collected by the hemispherical analyzer and their energies measured.

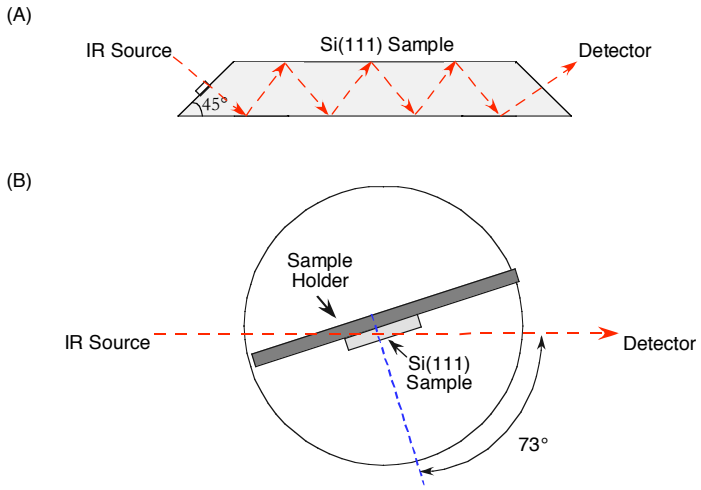

Figure 2.10 (A) A schematic of the multiple internal reflection (MIR) geometry for infrared absorption measurements. The silicon sample is beveled to allow entrance and exit of the light. (B) The transmission geometry for infrared absorption measurements. The sample is placed at a 73° angle to the surface normal. The IR radiation passes through the sample and is collected at the detector.

A Surface Science Instruments X-Probe spectrometer (SSX-100) was used for XPS measurements. Functionalized samples were loaded into a ultrahigh vacuum chamber and evacuated to a pressure $< 2\times10^{-9}$ Torr. The SSX-100 uses a monochromatic Al Kα x-ray source at an energy of 1486.6 eV and a SSI position-

sensitive electron detector. X-rays are incident at an angle of 55° to the surface normal. The incident spot size can be varied from 150 μm to 800 μm, which leads to energy resolutions varying from 0.8 eV to 1.8 eV, respectively. Emitted electrons are collected at an angle of 55° to the surface normal by a hemispherical energy analyzer. The pass energy of the analyzer can be varied between 25 V and 150 V, with the highest resolution being obtained at a pass energy of 25 V.

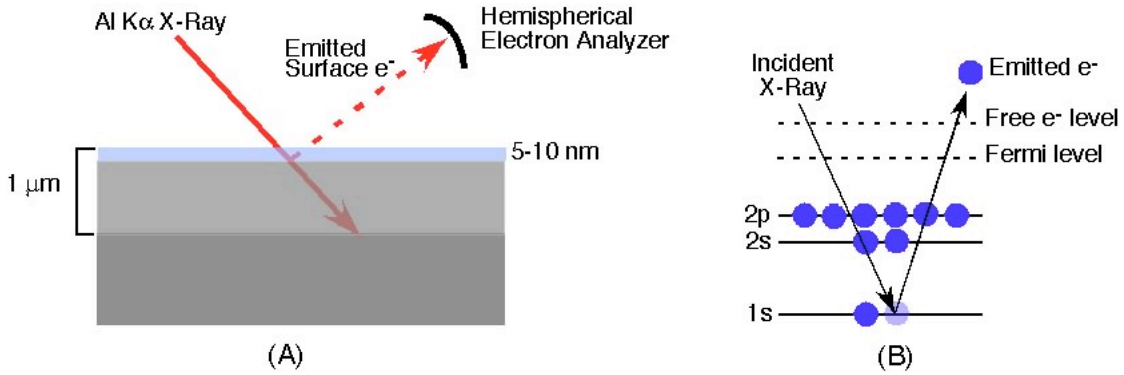

Figure 2.11 Schematic representation of the x-ray photoelectron spectroscopy. (A) An x-ray excites electrons up to a depth of 1 μm (shown in light grey), but only electrons in the top 5-10 nm (shown in light blue) of the sample are able to escape. These electrons are collected at an electron analyzer; (B) Energy diagram showing the excitation of core electrons in XPS.

An XPS survey scan is used to identify the elements present in the near-surface region of a sample. For example, in Fig 2.12 (A) four XPS peaks and one Auger peak (O KLL) are observed in the survey scan. Each peak corresponds to electrons emitted from a particular core shell of an element. In this case, silicon, oxygen, and carbon are all present at the surface. The atomic percent, a measure of the amount of an element present in the near-surface region, is calculated by dividing the signal intensity by a sensitivity factor determined by the spectrometer manufacturer.

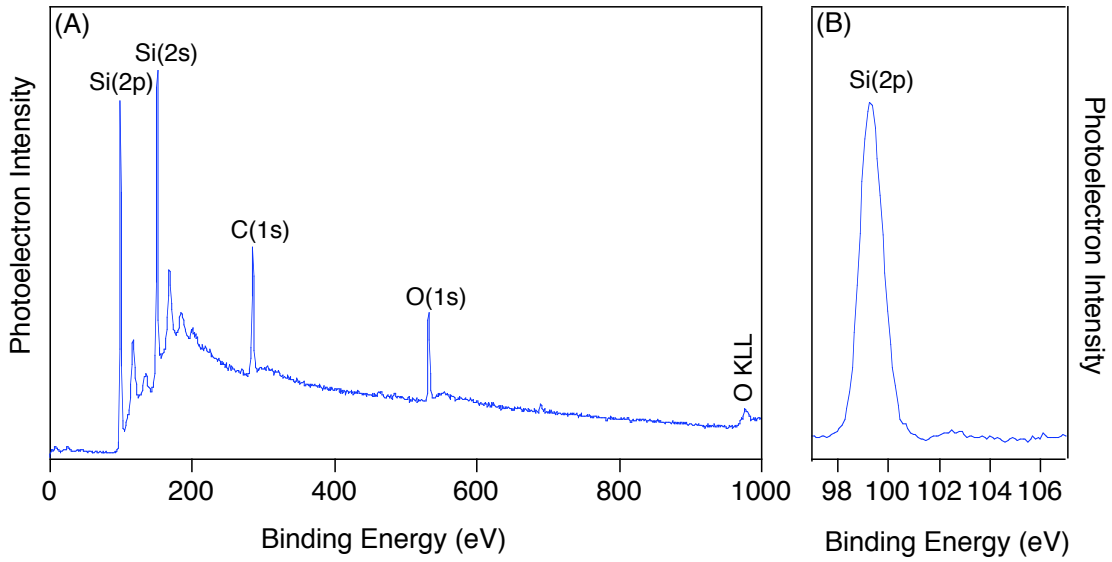

Figure 2.12 Representative XPS data. (A) Survey scan showing the presence of silicon, carbon and oxygen on the sample surface; (B) High-resolution scan of the silicon 2*p* region.

Figure 2.12 (B) is an example of a high resolution Si (2*p*) scan. The different chemical states for silicon can be studied using this spectrum. When sub-oxides of silicon are present at the surface, along with the main peak at 99.69 eV (Si^0), distinct transitions corresponding to the Si^{3+} (102.72 eV) and Si^{4+} (103.67 eV) species can be observed [18].

REFERENCES

1. Y. Wang, J. A. Henry, A. T. Zehnder, and M. A. Hines, *J. Phys. Chem. B* **107**, 14270 (2003).

2. H. Ford, *Advanced Mechanics of Materials* (Wiley, New York, 1963).

3. W. Kern and D. Puotinen, *RCA Rev* **31**, 187 (1970).

4. P. Jakob, P. Dumas, and Y. J. Chabal, *Appl. Phys. Lett.* **59**, 2968 (1991).

5. D. Halliday, R. Resnick, and J. Walker, *Fundamentals of Physics* (John Wiley & Sons 2003).

6. J. Flidr, Y.-C. Huang, and M. A. Hines, *J. Chem. Phys.* **111**, 6970 (1999).

7. R. A. Wind, H. Jones, and M. A. Hines, *J. Phys. Chem. B* **106**, 1557 (2002).

8. B. Yurke, D. S. Greywall, A. N. Pargelis, and P. A. Busch, *Phys. Rev. A* **51**, 4211 (1995).

9. D. S. Greywall, B. Yurke, P. A. Busch, A. N. Pargellis, and R. L. Willet, *Phys. Rev. Lett.* **72**, 2992 (1994)

10. Y. Wang, J. A. Henry, D. Sengupta, and M. A. Hines, *Appl. Phys. Lett.* **85**, 5736 (2004).

11. M. B. Smith, and J. March, *Advanced Organic Chemistry – Reaction Mechanisms, and Structure* (John Wiley & Sons, Inc., 2001).

12. H. C. Kolb, M. G. Finn, and B. K. Sharpless, *Angew. Chem. Int. Ed.* **40**, 2004 (2001).

13. A. Bansal, X. Li, I. Lauerman, and N. S. Lewis, *J. Am. Chem. Soc.* **118**, 7225 (1996).

14. L. J. Webb and N. S. Lewis, *J. Phys. Chem. B* **107**, 5404 (2003).

15. T. W. Greene and P. G. M. Wuts, *Protective Groups in Organic Synthesis* (John Wiley & Sons, 1991).

16. M. E. Jung, W. A. Andrus, and P. L. Ornstein, *Tetrahedron Lett.* 4175 (1977).

17. L. Yang, Y.-Y. Lua, M. Tan, O. A. Scherman, R. H. Grubbs, J. N. Harb, R. C. Davis, and M. Linford, *Chem. Mater.* **19**, 1671 (2007).

18. F. J. Grunthaner, P. J. Grunthaner, R. P. Vasquez, B. F. Lewis, and J. Maserjian, *Phys. Rev. Lett.* **43**, 1683 (1979).

Chapter 3

Mechanical Properties of Alkyl-Terminated Resonators

3.1 Introduction

The application of micromechanical resonators in the field of force and mass detection is based on the small changes in the resonant frequency that result from the adsorption of mass or the application of an external force. As shown by Ekinci *et al.* [1], the sensitivity of a resonator to small changes in adsorbed mass, δM, depends on the size of the resonator, and hence its effective mass, M_{eff}, as well as the quality factor, Q, of the device and its frequency of oscillation, f, by

$$\delta M \propto \frac{M_{eff}}{\sqrt{Q \times f}} \tag{3.1}$$

The ultimate sensitivity of resonators, thus depends to a large extent on a parameter that is not well understood – the quality factor of the resonator. In the simplest terms, Q is approximately the number of times a resonator will oscillate after an impulsive excitation before coming to rest. In an ideal world, a resonator would vibrate forever. In the real world, though, mechanical energy dissipation damps the oscillator's vibration and leads to a finite oscillation time. The quality factor is inversely related to mechanical energy dissipation and is defined to be

$$Q = \frac{2\pi E}{\Delta E} = \sqrt{1+\sqrt{2}}\,\frac{f}{\Delta f}, \tag{3.2}$$

where E is the total energy of the resonator, ΔE is the mechanical energy dissipated per cycle of oscillation, f is the resonant frequency of oscillation, and Δf is the full width of a Lorentzian resonant response curve at half the maximum amplitude.

In the quest for ultimate mass sensitivity, the size of micromechanical devices has been continuously decreasing. As devices get smaller, researchers have noticed an anti-correlation between the size of the resonator and its Q – smaller resonators having lower Q's than larger resonators. This puzzling trend has led to a number of hypotheses regarding the connection between Q and the surface of the resonator. Carr *et al.* demonstrated the relation between Q and the surface to volume ratio of 100-nm-thick and 200-nm-thick silicon cantilevers [2]. There was no change in this relation with a change in the thickness of the cantilevers. They hypothesized that it was the surface that was contributing to mechanical energy dissipation. Furthermore, Yang *et al.* demonstrated that annealing ultra-thin silicon cantilevers at 600-1000°C in the UHV chamber led to improvements in Q values [3]. They attributed their observed improvements in Q to reduced surface stress as a result of surface cleaning.

Mechanical energy dissipation in resonators terminated with different surface chemistries was studied. Wang *et al.* showed that changing a single monolayer on the surface – a change of less than 0.07% of the total mass – of a 5-μm-wide, 250-nm-thick silicon resonator resulted in a 70% change in Q [4, 5]. It was further shown that terminating silicon resonators with methyl moieties resulted in a six-fold improvement in the value of Q as compared to chemical-oxide-terminated resonators. These experiments also demonstrated that mechanical energy dissipation in the functionalized resonators scaled with the surface-to-volume ratio of the devices [6]. In other words, as the micromechanical devices got smaller, the surface-induced mechanical energy increased.

In this chapter, MHz-frequency silicon resonators terminated with alkyl groups of varying lengths were studied. If dissipation within the monolayer were significant, increasing the chain length would lead to increased mechanical energy dissipation and

decreasing *Q*. Interestingly, a very different dependence on chain length was actually observed.

3.2 Experimental

MHz-frequency silicon micromechanical resonators such as the one shown in Fig. 2.1 were fabricated from single-crystal silicon (111) wafers using standard lithography, reactive ion etching and wet chemical etching processes as described in Ch. 2. The doubly clamped resonators consisted of a hexagonal mass (measuring 4.2 μm, 5.7 μm, and 7.2 μm across the flats) and two 4-μm-long, 440-nm-wide supporting beams. The resonators varied in thickness between 350 nm and 425 nm depending on the final etching process. Depending on size, 77-84% of the surface of the resonator consisted of {111} planes.

Two different functonalization reactions were used to terminate the resonator surfaces with alkyl groups. In the first, a terminal alkene was reacted with a H-terminated surface [7]. In the second, a H-terminated resonator was first chlorinated by exposure to Cl_2 (g) under UV irradiation. The Cl-terminated resonator was then immersed in the appropriate Grignard reagent [8]. Both of these procedures were described in detail in Ch. 2.

After functionalization, the resonators were loaded into an ion-pumped vacuum chamber (10^{-8} Torr base pressure). The dynamical mechanical properties of the resonators were periodically measured using the non-invasive laser interferometric system described in Ch. 2. The resonators were removed from vacuum and placed in a sealed container filled with room air at 100% humidity. After a few days, the resonators were removed from the container, placed in the vacuum chamber and retested.

The small size of the resonator samples precluded their direct spectroscopic interrogation. To characterize the functionalization process, larger samples were co-processed with the resonators. Immediately after functionalization, these samples were loaded into an FTIR spectrometer and analyzed. This process is described in greater detail in Ch. 2.

3.3 Results

3.3 (i) Surface Characterization

3.3 (i) (A) Characterization of Monolayer Quality

The chemical composition of the functionalized surfaces was characterized using infrared absorption spectroscopy in the multiple internal reflection (MIR) geometry. Over the range of 1500-4000 cm^{-1}, the spectrum was featureless except in the 2800-3000 cm^{-1} range, which is the characteristic region for C–H stretch vibrations. Fig 3.1 compares the infrared absorption spectra from dodecyl- and octadecyl-terminated surfaces prepared by the hydrosilylation method [7]. The three prominent absorption bands correspond to the symmetric and antisymmetric CH_2 stretch vibrations at 2850 and 2921 cm^{-1} respectively, and the CH_3 symmetric stretch at 2975 cm^{-1} As expected, the CH_3 bands of the octadecyl and dodecyl-terminated surfaces have comparable intensity. In contrast, the CH_2 bands corresponding to the octadecyl-terminated surface are approximately 50% more intense than those corresponding to the dodecyl-terminated surface. The higher intensity of the octadecyl monolayer spectrum is a result of the larger length of the octadecyl moiety, resulting in a 50% increase in the number of C–H bonds in the monolayer.

The energy of the antisymmetric CH_2 stretch mode can be used as an indicator of monolayer density and packing. For example, this peak shifts 6-8 cm^{-1} towards lower energy as bulk alkanes undergo a liquid-to-crystal transition [9]. In this experiment, the energy of the CH_2 antisymmetric stretch mode was 2920.4 cm^{-1} for both the dodecyl- and octadecyl-terminated surfaces, which is slightly lower than the previously reported value of 2921 cm^{-1} for well-ordered monolayers [7]. From this, we concluded that both monolayers had comparable packing.

3.3 (i) (B) The Effect of Two Different Synthetic Strategies on Monolayer Quality

Two different synthetic strategies – hydrosilylation and the two-step Grignard reagent reaction – may be used to terminate silicon surfaces with organic monolayers. The effect of the synthetic strategy used on the quality of the monolayers was characterized using infrared spectroscopy.

Figure 3.2 shows the C-H stretch region of infrared spectra corresponding to dodecyl-terminated surfaces functionalized with two different synthetic strategies. One surface was prepared using the hydrosilylation method (red trace), whereas the other was prepared using the Grignard–reagent method (blue trace). The two spectra have nearly identical absolute intensity and peak positions. Additionally both surfaces have an antisymmetric stretch mode ay 2924 cm^{-1}, indicative of dense packing. These results suggest that the two synthetic strategies produce monolayers of comparable quality.

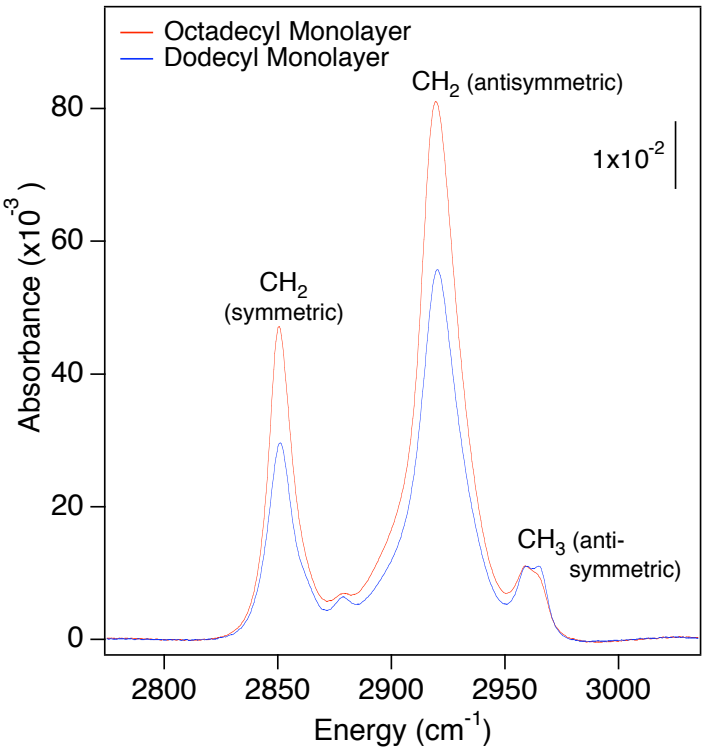

Figure 3.1 Infrared absorption spectra collected in the multiple reflection geometry showing the C–H stretching region for dodecyl- and octadecyl-terminated surfaces prepared using the hydrosilylation method. The antisymmetric CH_2 peak for both monolayers was observed at 2920.4 cm^{-1}, indicating the formation of well-ordered monolayers.

3.3 (i) (C) The Effect of Three Different Solvents on Monolayer Quality

Most reactions used for functionalizing silicon surfaces involve the use of organic solvents at elevated temperatures. To study the effect of organic solvents at elevated temperatures on the quality of the resulting monolayers, a series of experiments were performed.

In the first experiment, Cl-terminated silicon samples, prepared as described in Sect. 2.4(ii), were refluxed in diethyl ether for 2 hours at ~67°C in an inert atmosphere. At the end of two hours, dodecyl Grignard reagent was added to the

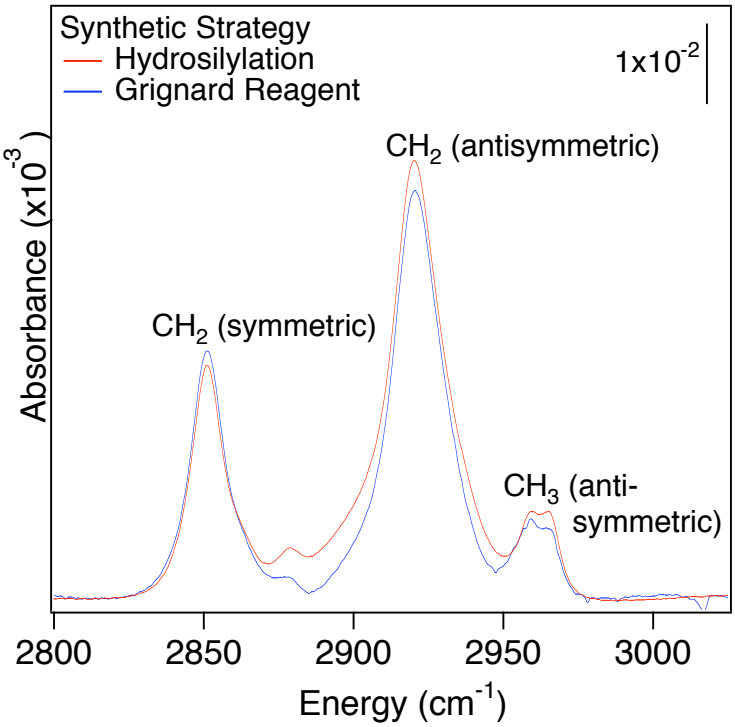

Figure 3.2 Infrared absorption spectra collected in the multiple reflection geometry showing the C–H stretching region for dodecyl-terminated surfaces. The red trace corresponds to the hydrosilylation method of monolayer preparation, whereas the blue trace corresponds to the Grignard reagent method. Similar intensity and antisymmetric CH_2 peak positions are indicative of monolayer quality being independent of synthetic strategy.

reaction vessel and the samples refluxed for a further 48 hours in an inert atmosphere. In the second experiment, Cl-terminated silicon samples were refluxed in diglyme for 2 hours at ~167°C in an inert atmosphere. At the end of two hours, dodecyl Grignard reagent was added to the reaction vessel and the samples refluxed for a further 48 hours in an inert atmosphere. In the third experiment, Cl-terminated samples were refluxed in tetrahydrofuran for 2 hours at ~167°C in an inert atmosphere. At the end of two hours, octadecyl Grignard reagent was added to the reaction vessel and the

samples refluxed for a further 48 hours in an inert atmosphere. In the last experiment, Cl-terminated samples were refluxed in diglyme for 2 hours at ~167°C in an inert atmosphere. At the end of two hours, octadecyl Grignard reagent was added to the reaction vessel and the samples refluxed for a further 48 hours in an inert atmosphere.

At the end of each experiment the samples were rinsed successively in methylene chloride and ultrapure water, followed by surface characterization. The surfaces resulting from the above experiments were compared to dodecyl- and octadecyl-terminated surfaces prepared as described in Sect. 2.4(i).

Fig 3.3 demonstrates the effect of organic solvents at elevated temperatures on dodecyl-terminated surfaces. The C–H stretching region of a well-ordered dodecyl-monolayer has an antisymmetric CH_2 absorption at 2921.1 cm^{-1}. The position of this CH_2 peak shifts by ~4 cm^{-1} to a lower energy when the surface is refluxed in diglyme, whereas there is no effect upon refluxing in ether. The lower intensity of the peaks for the diglyme experiment further confirms that exposure to solvent deleteriously effects surface coverage and lowers the quality of the monolayer.

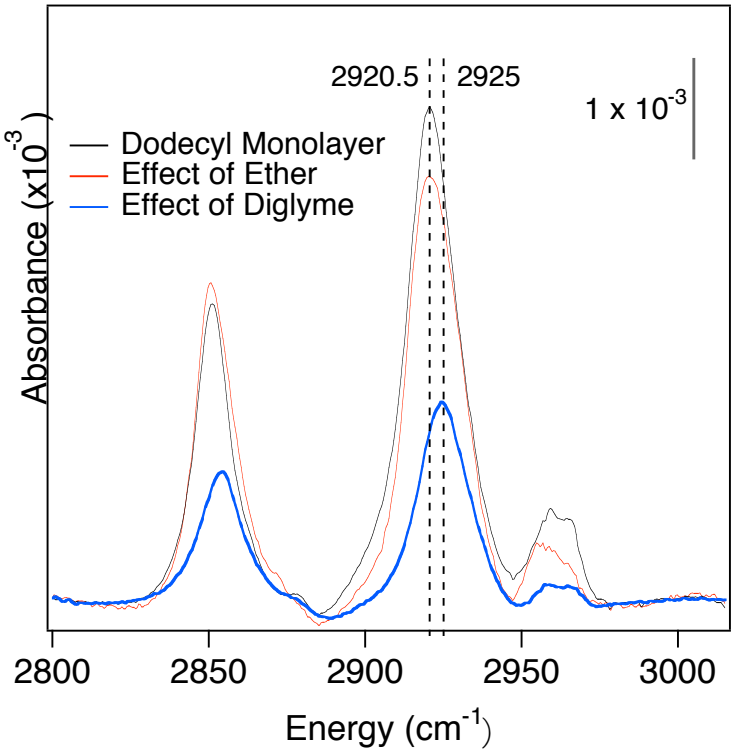

Figure 3.3 Infrared absorption spectra, collected in multiple internal geometry, showing the C–H stretch region of dodecyl-terminated Si(111) surfaces. Refluxing the Cl-terminated silicon surfaces in diglyme before refluxing in dodecyl Grignard reagent has a deleterious effect on monolayer quality, as is shown by the blue shift of the antisymmetric CH_2 peak (shown with the dotted lines). No such effect is observed when the Cl-terminated surfaces are refluxed in diethyl ether before refluxing in the Grignard reagent.

The effect of organic solvents at elevated temperatures on octadecyl-terminated surfaces is shown in Fig. 3.4. For the octadecyl-terminated surface, the peak position of the antisymmetric CH_2 stretch is at 2921.4 cm^{-1}. In comparison, refluxing silicon surfaces in either THF or diglyme before exposure to octadecyl Grignard reagent results in a blue shift of ~3 cm^{-1} for the antisymmetric CH_2 peak. The low intensity of the signals corresponding to the THF- and diglyme-exposed surface, as well as the corresponding blue shift, shows that exposure to these solvents

at elevated temperatures results in monolayers with lower surface coverage and quality.

As demonstrated by the position of the antisymmetric CH_2 stretch in Figs. 3.3 and 3.4, the following trend is observed in the effect of solvents on monolayer quality,

ether < THF < diglyme.

This trend also correlates with the temperatures at which the three solvents reflux, i.e.,

67°C (ether) < 67°C (THF) < 120°C (diglyme).

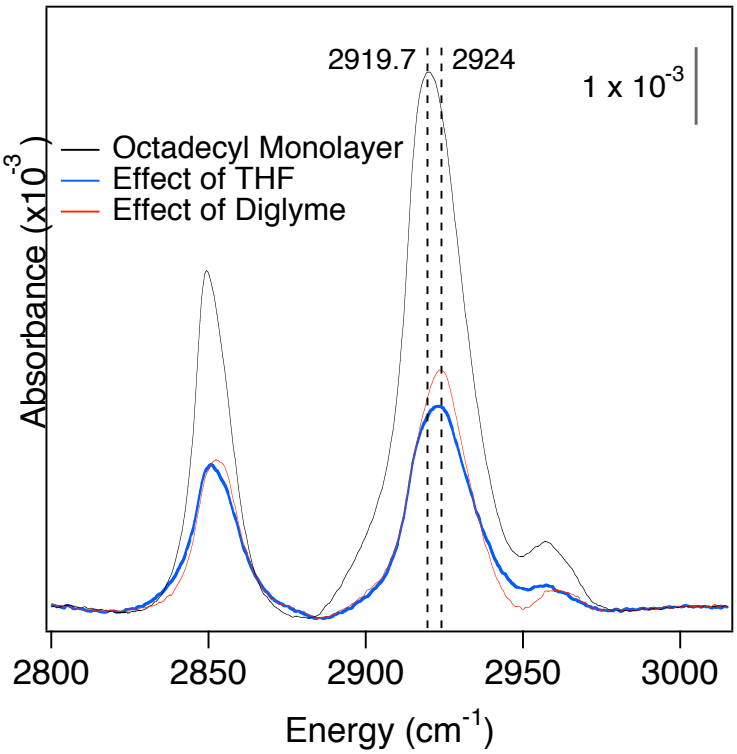

Figure 3.4 Infrared absorption spectra, collected in the multiple internal reflection geometry, showing energy corresponding to the C-H stretch for octadecyl-terminated Si(111) surfaces. Refluxing the Cl-terminated silicon surfaces in diglyme or THF before refluxing in octadecyl Grignard reagent has a deleterious effect on monolayer quality, as is shown by the blue shift of the antisymmetric CH_2 peak (shown with the dotted lines) when compared to the octadecyl-terminated surface prepared using the method described in Sect. 2.4(i).

3.3 (ii) Mechanical Property Measurements

3.3 (ii) (A) Effect of Two Different Synthetic Strategies on *Q*

The two different methods used for preparing long-chain-alkyl monolayers involve very different chemistries. Although the spectroscopic investigations in the last section showed that the two strategies produced chemically similar monolayers, there are undoubtedly subtle differences between the two preparations. For example, the chlorine-termination step (which is required for the Grignard-reagent reaction) is known to roughen the silicon substrate [10, 11]. Do these subtle differences affect the mechanical performance of functionalized resonators?

To answer this question, dodecyl-terminated resonators were prepared using both strategies. Figure 3.5 compares the frequencies and quality factors of three sizes of resonators prepared using hydrosilylation (red) and Grignard-reagent-based (blue) syntheses. No systematic difference between the two methods is seen, suggesting that the synthetic strategy has no substantive effect on mechanical energy dissipation.

3.3 (ii) (B) The Effect of Alkyl Chain Length on *Q*

In functionalizing surfaces with organic monolayers, the resonators are terminated with alkyl groups consisting primarily of CH_2 groups. These alkyl groups can be compared to simple waxes, such as paraffin, which are bulk alkanes comprising of CH_2 moieties. Intuitively, paraffin is expected to be highly dissipative. Would a resonator terminated with an organic moiety similar to paraffin be as dissipative? To study the dissipation in the monolayer itself, silicon resonators were terminated with alkyl groups of various chain lengths and the mechanical properties of the resonator studied.

To answer this question, the effect of alkyl chain length on mechanical properties was studied. The rate of mechanical energy dissipation within the monolayers should increase linearly with chain length (*i.e.*, with increasing film thickness), whereas mechanical energy dissipation at the Si/alkyl or alkyl/vacuum interfaces should be independent of chain length.

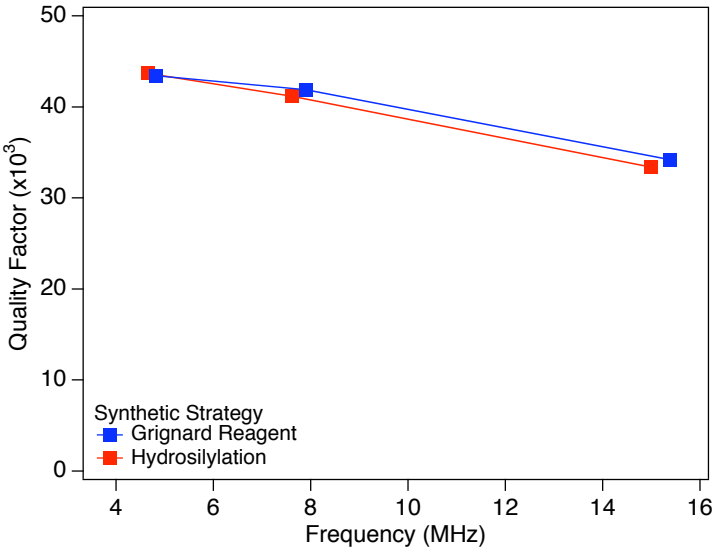

Figure 3.5 A comparison of the mechanical properties of dodecyl-terminated resonators functionalized using the hydrosilylation (red) or Grignard-reagent-based (blue) synthetic strategies.

The effect of alkyl chain length on the quality factor of 7.2-μm-wide resonators is shown in Fig. 3.6. (Other resonator sizes showed similar trends.) The quality factors of long-chain-alkyl (C_nH_{2n+1}, $n \geq 2$) terminated resonators are essentially independent of chain length. Increasing the length of the chain by almost an order of magnitude (*i.e.* from C_2H_5 to $C_{18}H_{37}$) actually leads to slight improvement of Q (*i.e.*, a decrease in the rate of mechanical energy dissipation). Interestingly, methyl-terminated resonators have much better performance than long-chain-alkyl terminated devices.

This result indicates that mechanical energy dissipation within the monolayer is negligible in comparison to the total mechanical energy dissipation in the device. If dissipation within the monolayer were the dominant source of energy loss, increasing the length of the alkyl chain from C_2 to C_{18} – a nine-fold increase – would result in a nine-fold decrease in Q.

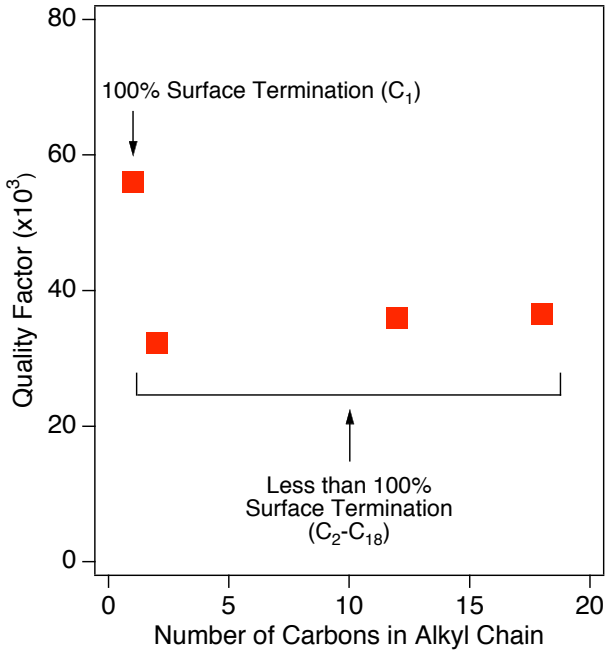

Figure 3.6 The dependence of quality factor on the chain length for 7.2-µm-wide alkyl terminated resonators. The highest quality factors are observed for methyl-terminated resonators, whereas resonators with other alkyl-terminations have a quality factor which is at least 50% lower.

3.3 (ii) (C) Long-Term Stability of Alkyl-Terminated Resonator

The long-term stability of alkyl-terminated resonators was studied in both air and vacuum, as shown in Fig. 3.7 for 7.2-µm-wide resonators. (Other resonator sizes showed similar trends.) During the first 72 hours of measurement, the resonators were stored at 10^{-8} Torr while their mechanical properties were periodically measured.

During this period, no systematic change in Q was observed. On average, the methyl-terminated

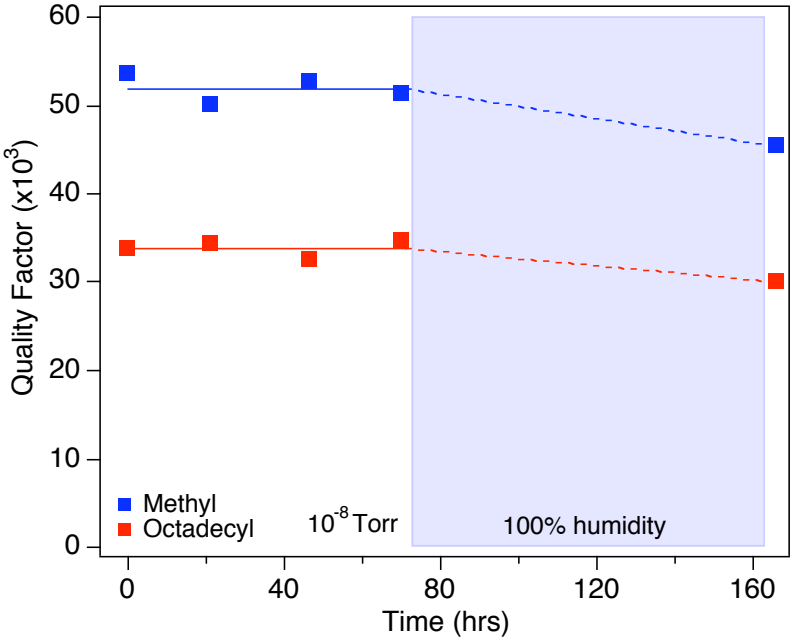

Figure 3.7 The time dependant behavior of 7.2-µm-wide resonators terminated with octadecyl (red squares) and methyl (blue squares) moieties. The quality factor of the resonators remains constant over ~72 hours in vacuum. On exposure to water-saturated air, the quality factor decreases by ~12% for both methyl- and octadecyl-terminated resonators.

resonators had Q ~52000, whereas resonators terminated with longer alkyl chains had Q ~34000. After 72 hours the resonators were removed from vacuum and placed in a sealed atmosphere saturated with 100% humidity for 96 hours. The resonators were then returned to the vacuum chamber and their properties measured. As shown in Fig. 3.7, both sets of paddles displayed a small (~12%) decrease in Q after the process.

Previous results have shown that the mechanical properties of H-terminated resonators degrade rapidly with time, even at a pressure of 10^{-8} Torr [4]. Thus, the long-term-stability observed for alky-terminated resonators is a marked improvement

over hydrogen-terminated resonators. Interestingly, this improvement is independent of surface termination. Methyl- and long-chain-alkyl-terminated resonators displayed similar stabilities in both air and vacuum.

3.4 Discussion

The magnitude of chemically induced mechanical energy dissipation in micromechanical resonators is rather surprising. Changing the termination of the resonator surface from methyl to longer alkyl moieties, a change of a single monolayer, results in a 50% change in the mechanical energy dissipation of the resonator! The data for alkyl-terminated resonators can be used to calculate a lower bound for the rate of the observed mechanical energy dissipation and to account for the difference in mechanical energy dissipation observed for resonators terminated with different alkyl-chain-lengths. Assuming that no dissipation takes place at the silicon-alkyl interface in methyl-terminated resonators, the Q of methyl-terminated resonators, Q_{methyl}, will depend only on the dissipation due to clamping and bulk losses. (There will be no viscous drag losses because the resonators are operated in vacuum.) Thus,

$$\frac{1}{Q_{methyl}} \propto \gamma_{clamping} + \gamma_{bulk} \tag{3.1}$$

where γ_{clamping} and γ_{bulk} is the mechanical energy dissipation due to clamping losses and bulk losses, respectively. For resonators terminated with alkyl moieties larger in size than methyl, a lower Q (*i.e.*, higher mechanical energy dissipation) is observed. Assuming that all other conditions are kept constant, the additional energy dissipation at those surfaces can be attributed to the silicon-alkyl interface. Consequently, the corresponding Q of long-chain-alkyl-terminated resonators, Q_{alkyl}, will be given by

$$\frac{1}{Q_{alkyl}} \propto \gamma_{clamping} + \gamma_{bulk} + \gamma_{interface}, \tag{3.2}$$

where $\gamma_{interface}$ is the dissipation at the silicon-alkyl interface. The contribution of the interface towards the mechanical energy dissipation in the resonator is then given by

$$\frac{\gamma_{interface}}{\gamma_{clamping} + \gamma_{bulk} + \gamma_{interface}} = 1 - \frac{Q_{alkyl}}{Q_{methyl}}. \tag{3.3}$$

By applying the above relationship to the quality factor obtained for methyl-, ethyl-, dodecyl- and octadecyl-terminated resonators, we find that the ethyl-silicon interface has the most contribution to mechanical energy dissipation, contributing as much as 47% to the total mechanical energy dissipation of the resonator. On average the contribution of the Si-alkyl interface towards energy dissipation is approximately 40%.

In this chapter we have tried to explore the origins of the difference between the mechanical energy dissipation in methyl-terminated and longer-alkyl-terminated resonators. A number of possible theories have been studied to determine a possible cause for mechanical energy dissipation in alkyl-terminated resonators. Firstly, the dissipation in the monolayer itself has been shown to be negligible. A 9-fold increase the length of the alkyl chain would be expected to result in a corresponding increase in mechanical energy dissipation, which is not observed. In fact, the *Q*'s slightly increase with increasing chain length of the alkyl moieties. Secondly, dissipation does not depend on the bonds at the silicon–monolayer interface. If the interface bonds were contributing to mechanical energy dissipation, then the ethyl-terminated surface, having 50% Si-C and 50% Si-H termination should have *Q*'s intermediate between those observed for methyl- and H-terminated resonators. This in not what is observed. The *Q*'s for H-terminated resonators lie in-between the values observed for methyl-

and longer-alkyl-terminated resonators. Thirdly, the chemical method used for surface termination does not effect the quality of the monolayer or value of *Q*. Characterization of the surface after monolayer formation using two different synthetic strategies (*i.e.*, hydrosilylation and the Grignard reagent method) showed that there was no perceptible difference between the quality of the resulting monolayers. Furthermore, the Q for the resulting monolayer-terminated resonators are also similar.

An alternate theory for mechanical energy dissipation could be due to electronic defects at the surface of the resonators. In high purity float zone silicon, the density of electronically active bulk defects is extremely low and hence recombination of excited carriers occurs exclusively at surface defects. Thus, measuring the charge carrier lifetimes of different surfaces provides a measure of the density of electronic defects at the surface – less electronic defects resulting in longer charge carrier lifetimes. The characterization of the surface electronic defects of different alkyl-terminated Si(111) surfaces shows that methyl-termination results in a low density of electronic defects, with the number of defects increasing very slowly with time [13]. In comparison, the longer-alkyl-terminated surfaces have almost twice the electronic defect density as compared to methyl-terminated surfaces [14]. The trend in mechanical energy dissipation in the various monolayers,

$$\text{long alkyl} > \text{H} > \text{CH}_3,$$

follows the trend observed in the density of electronic defects on these surfaces. (The mechanical dissipation in H-terminated resonators, and its long-term stability, has been reported previously [4].) The trend in the long-term performance of these surfaces,

$$\text{H} > \text{long alkyl} > \text{CH}_3,$$

also mirrors the trend for the increase in surface electronic defects over time. (Yablonovitch *et al.* [15] have previously characterized the increase in electronic defects on a H-terminated surface over time.)

Even though the mechanical energy dissipation can be attributed to surface electronic defects, the chemical nature of these surface defects is still unclear. It has been suggested, however, that alkyl-terminated surfaces prevent the formation of surface electronic defects by controlling the oxidation of the surface [9]. Although the alkyl-terminated surface are significantly oxidized on prolonged exposure to air, the oxide that is formed consists mainly of suboxide species having lower density of electronic defects [16]. This is in sharp contrast to H-terminated resonators, on which oxide layers of poor quality are formed, the oxide having a greater density of electronic defects.

The *Q* can also be correlated to the density of the alkyl monolayer. The van der Waals' diameter for methyl is 2.5Å [17], whereas the distance between two adjacent Si(111) surface sites is 3.8Å [18]. The smaller size of the methyl moieties would enable the attachment of a methyl moiety to each and every site on the Si(111) surface. On the other hand, the van der Waals radius of an alkyl moiety having more than 2 carbons is ~4.5-5Å [19]. The size of the larger alkyl moieties prevents the attachment of these moieties to every surface site. At most 50% of the surface sites will be occupied by alkyl moieties with more than two carbons [20].

3.5 Conclusion

Chemistry at the surface of silicon resonators plays an important role in mechanical energy dissipation. Significantly higher *Q* values are observed for methyl-terminated-MHz-frequency silicon oscillators as compared to similar resonators

terminated with longer alkyl moieties. The Q of the resonators terminated with longer alkyl moieties were in turn higher than those for H-terminated resonators. The better performance of alkyl-terminated resonators is attributed to lower electronic defect densities in the monolayer-coated-resonators as well as the passivity of the resonator surface to chemical attack.

REFERENCES

1. K. L. Ekinci, Y. T. Yang, and M. L. Roukes, *J. Appl. Phys.* **95**, 2682 (2004).

2. D. W. Carr, S. Evoy, L. Sekaric, H. G. Craighead, and J. M. Parpia, *Appl. Phys. Lett.* **75**, 920 (1999).

3. J. Yang, T. Ono, and M. Esashi, *Appl. Phys. Lett.* **77**, 3860 (2000).

4. J. Henry, Y. Wang, and M. A. Hines, *Appl. Phys. Lett.* **84**, 1765 (2004).

5. Y. Wang, J. A. Henry, D. Sengupta, and M. A. Hines, *Appl. Phys. Lett.* **85**, 5736 (2004).

6. Y. Wang, J. A. Henry, A. T. Zehnder, and M. A. Hines, *J. Phys. Chem. B* **107**, 14270 (2003).

7. M. R Linford, P. Fenter, P. M. Eisenberger, and C. E. D. Chidsey, *J. Am. Chem. Soc*. **117**, 3145 (1995).

8. A. Bansal, X. Li, I. Lauerman, and N. S. Lewis, *J. Am. Chem. Soc.* **118**, 7225 (1996).

9. R. G. Snyder, H. L. Strauss, and C. A. Elinger, *J. Phys. Chem.* **86**, 5245 (1982).

10. B. J. Eves and G. P. Lopinski, *Surface Science* **579**, 89 (2005).

11. G. P. Lopinski, B. J. Eves, O. Hul'ko, C. Mark, S. N. Patitsas, R. Boukherroub, and T. R. Ward, *Physical Review B* **71**, 4 (2005).

12. F. R. Blom, S. Bowstra, M. Elwenhoek, and J. H. J. Fluitman, *J. Vac. Sci. Technol. B*, **10**, 19 (1992).

13. W. J. Royea, A. Juang, and N. S. Lewis, *Appl. Phys. Lett.* **77**, 1988 (2000).

14. L. J. Webb and N. S. Lewis, *J. Phys. Chem. B* **107**, 5404 (2003).

15. E. Yablonovitch, D. L. Allara, C. C. Chang, T. Gmitter, and T. B. Bright, *Phys. Rev. Lett.* **57**, 249 (1986).

16. L. J. Webb, D. Michalak, J. S. Biteen, B. S. Brunschwig, A. S. Y. Chan, D. W. Knapp, H. M. Meyer, III, E. J. Nemanick, M. C. Traub, and N. S. Lewis, *J. Phys. Chem. B* **110**, 23450 (2006).

17. A. Fidelis, F. Ozanam, and J. N. Chazalviel, *Surf. Sci.* **444**, L7 (2000).

18. S. M. Sze, *The Physics of Semiconductor Devices*, 2nd Ed. Wiley, NY (1981).

19. A. B. Seival, B. v. d. Hout, H. Zuilhof, and E. J. R. Sudholter, *Langmuir* **17**, 2172 (2001).

20. A. B. Sieval, B. v. d. Hout, H. Zuilhof, and E. J. R. Sudholter, *Langmuir* **16**, 2987 (2000).

Chapter 4

Acetal/Methyl-Terminated Resonators – The Perils of Using Protecting Groups on Resonant Devices

4.1 Introduction

One of the potential applications for micromechanical resonators is as the active element in high performance chemical and biological sensors. In this application, a small applied mass [1] (or force [2]) leads to a shift in the resonant frequency of a micromechanical resonator. To make the sensor specific to a particular analyte, the surface of the resonator must be functionalized with a molecule that specifically binds to the analyte of interest. The key challenge lies in introducing the required functionality without degrading the mechanical properties of the device.

One strategy for introducing sensing functionalities to the resonator surface is to use a protected functional group. In this method, a "protected" version of the sensing motif is first attached to the surface, then the sensing functionality is "deprotected" using a second chemical reaction. This strategy is potentially useful for the attachment of silicon-reactive motifs. For example, alcohols and aldehydes have been shown to directly react with hydrogen-terminated silicon surfaces [3] and hence cannot be used directly as sensing functionalities.

In this experiment, resonators were functionalized with one of the most common protecting groups – an acetal. This group can be converted to a number of different groups – including carboxylic acids, acetals, amines and cyano groups – using simple, well-understood chemical reactions [4]. Because of this flexibility, the

acetal group could serve as the starting point for the attachment of many different species.

As discussed in Ch. 1, one of the key requirements for high sensitivity detection is the use of high *Q* resonators. For reasons that are not well-understood, the quality factor of micromechanical resonators depends sensitively on the chemical state of the resonator's surface. For example, methyl-terminated MHz-frequency silicon oscillators have been shown to have high *Q* [5], whereas similar oxide-terminated devices have much poorer performance. Interestingly, methyl-terminated resonators have somewhat better *Q* than comparable long-chain-alkyl-terminated device (*e.g.* ethyl-, dodecyl-, or octadecyl-terminated resonators. Again, the reason for this difference is not completely understood, but it appears to be related to packing density. Steric effects limit the packing of long-chain-alkyl groups to (at most) 50% of Si(111) surface sites. In contrast, the smaller size of the methyl groups allows for 100% termination.

Since acetal groups are considerably larger than alkyl chains, a fully acetal-functionalized surface would be expected to have a very low packing density – far below the 50% packing found for long-chain-alkyl coatings. As such, the quality factors of acetal-functionalized resonators are likely to be low. To circumvent this problem, mixed monolayers displaying primarily methyl groups with a low density of acetal functionality were studied. We chose 1,3-dioxan-2-ylethyl as a prototypical acetal. The ethyl "tail" on this molecule elevates the acetal group above the methyl "carpet", while not allowing enough flexibility for collapse of the acetal onto the substrate. A cartoon of the mixed monolayer is shown in Fig. 4.1.

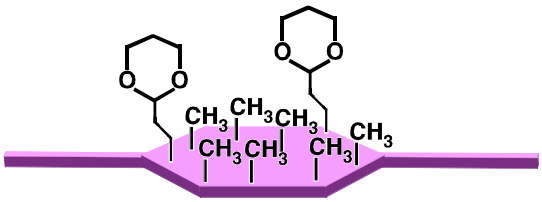

Figure 4.1 A cartoon of an acetal/methyl-terminated resonator. The chemistry shown is also present on the surface of the supporting beams.

4.2 Experimental

MHz-frequency silicon resonators, such as the one shown in Fig 2.1, were fabricated from single crystal Si(111) wafers at the Cornell NanoScale Science and Technology Facility as described in detail in Ch. 2. The resonators consisted of a central hexagonal paddle connected to the bulk by two 440-nm-wide and 4-μm-long supporting beams. Three different paddle widths (and thus three different nominal frequencies) were studied; the paddles measured 4.2 μm, 5.7 μm and 7.2 μm across the flats. The paddles and supporting beams had the same thickness, which varied over the range 350-425 nm, (calculated from resonant frequency) depending on the duration of the KOH etch. The resonator frequencies varied from 4 MHz to 17 MHz, depending on the size and thickness of the resonators. Depending on the size of the resonator, 74-87% of the exposed surface was composed of {111} faces.

A two-step synthesis, based on Grignard reagent chemistry [6], was used to form mixed 1,3-dioxan-2-ylethyl/methyl monolayers. The resonators were first H-terminated, following the procedure described in Sect. 2.2(v), and then chlorinated as described in Sect. 2.4(ii). Mixtures of methyl Grignard reagent (CH_3MgCl, 3.0 M in THF, Sure-Seal, Aldrich) and 1,3-dioxan-2-ylethyl Grignard reagent ($C_6H_{11}O_2MgBr$, 0.5 M in THF, Sure-Seal, Aldrich), ranging in concentration of 1,3-dioxan-2-ylethyl Grignard reagent from 0.02 M to 0.2 M, were prepared by cannulating required

amounts of the reagents into a measuring cylinder attached to the Schlenk line under a positive pressure of Ar. The Cl-terminated surfaces were then immersed in the mixed Grignard reagent under Ar and refluxed for 1.5 hours at ~67°C under a constant flow of Ar. At the end of the reaction, the reaction mixture was removed from inert atmosphere, diluted with THF and decanted. The samples were then rinsed with anhydrous methanol, methylene chloride and ultrapure water.

The transformation of the acetal to an aldehyde, as shown in Fig. 4.2, was achieved using three different chemical strategies. In the first strategy, the acetal/methyl- functionalized resonators were reacted with 1.0 M HCl for 30 min at 80°C, followed by thorough rinsing with ultrapure water [7]. In the second chemical reaction, the acetal/methyl-terminated resonators were immersed in 1.0 M CH_3COOH for 30 min at room temperature, followed by rinsing in ultrapure water [7]. The final was a non-aqueous reaction that used 1.0 M iodotrimethylsilane (TMSI) in chloroform [8] for deprotection. The TMSI ($(CH_3)_3SiI$, Aldrich, 97%) solution in chloroform was prepared by opening a 5 g vial of the chemical under inert atmosphere in an oxygen- and water-free glove box and transferring the contents to a round-bottom flask with a sealable side-arm. The TMSI was removed from the glove box under inert atmosphere and attached to a Schlenk line. A 1.0 M solution was prepared by cannulating 25 ml of chloroform into the flask under a positive pressure of Ar. The TMSI solution was then cannulated into the flask containing acetal/methyl-terminated samples under a positive pressure of Ar and the samples left to react with the TMSI under a constant flow of Ar for 15 min at room temperature. At the end of reaction, the samples were rinsed in methylene chloride and ultrapure water.

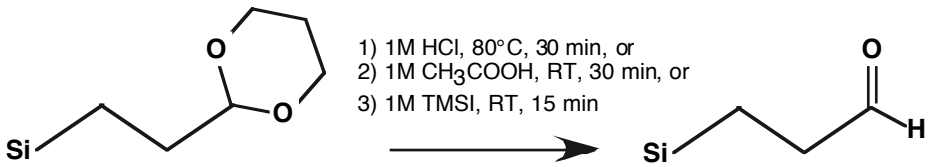

Figure 4.2 Reaction scheme showing the conversion of the acetal functionality to an aldehyde. Three different deprotection methods were tried.

To test the effect of the 80°C, 1.0 M HCl deprotection strategy on methyl-terminated sites – which were initially thought to be non-reactive to this chemical – a control reaction using methyl-terminated surfaces was performed. Methyl-terminated resonators were formed using the procedure in Sect. 2.4(ii). The methyl-terminated resonators were then reacted with 80°C, 1.0 M HCl for 30 minutes in air, followed by rinsing with ultrapure water.

For use as a reference in our spectroscopic studies, chemical-oxide-terminated silicon samples were prepared as follows [9]. Hydrogen-terminated surfaces were prepared using the procedure in Sect. 2.2 (v) and then exposed to ozone generated with a Hg pen-lamp in ambient atmosphere for 20 min, making sure to keep the surface of the sample in the line of sight of the lamp. This procedure resulted in the formation of ~13Å of SiO_2 on the surface [9]. After functionalization, the resonators were immediately loaded into a vacuum chamber for mechanical property testing or into an FTIR spectrometer for characterization of the functionalized silicon surface.

4.3 Results

4.3 (i) Surface Characterization: Acetal/Methyl-terminated surfaces

The chemical composition of the functionalized surfaces was studied using infrared spectroscopy in both the multiple-internal-reflection (MIR) and transmission geometries. Due to their extremely small size, direct characterization of the resonator surface was not possible. Instead, 0.59″×1.56″ Si(111) samples, processed simultaneously with the resonator samples, were characterized. For MIR measurements, the shorter sides of these silicon samples were beveled at 45° as described in Sect 2.5(i).

The C-H stretch region of the infrared spectrum of mixed acetal/methyl-functionlized surfaces taken in the MIR geometry is displayed in Fig. 4.3. The blue spectrum represents the initial surface, whereas the red trace was taken after deprotection with 80°C, 1 M HCl. The surfaces were prepared using a mixture of 2.7 M methyl- and 0.045 M acetal-Grignard reagents. For the acetal/methyl-terminated surface, the antisymmetric and symmetric CH_2 stretch peaks are at 2928 cm^{-1} and 2980 cm^{-1} respectively. After reaction with 1.0 M HCl at 80°C for 30 minutes, the conversion of the 1,3-dioxan-2-ylethyl moieties to aldehydes leads to a loss in intensity of both the antisymmetric and symmetric CH_2 stretch peaks. During the deprotection process the acetal moiety should lose three CH_2 groups, which would explain the decrease in intensity of both the CH_2 peaks in the infrared spectra.

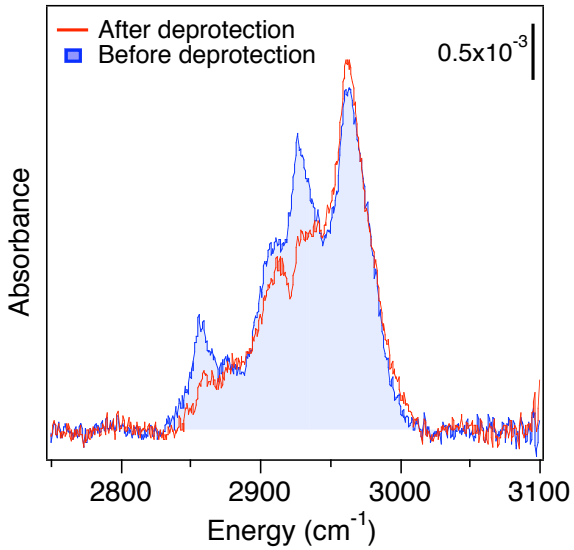

Figure 4.3 Infrared spectra for the 1,3-dioxan-2-ylethyl/methyl-terminated surface (blue trace) and the same surface after deprotection with 80°C, 1 M HCl (red trace). The initial 1,3-dioxan-2-ylethyl/methyl-terminated surface was prepared using a 0.08 M 1,3-dioxan-2-ylethyl and 2.5 M methyl Grignard reagents, and the infrared data were collected in the multiple internal reflection geometry. The energy region shown corresponds to C-H stretch vibrations.

For surfaces terminated with CH_2 groups, the position of the antisymmetric C–H stretch vibration of the CH_2 moiety can be used to ascertain the quality of the monolayer on the surface due to its sensitivity towards monolayer density. The energy of vibration for well-ordered, solid alkanes is 6-8 cm^{-1} less than that of less-ordered liquid alkanes [10]. For the present experiment, there is no perceptible change in the position of the antisymmertic CH_2 peak, which shows that there is no perceptible change in monolayer quality after deprotection.

Another energy region of interest in this experiment lies between 1600 cm^{-1} and 1800 cm^{-1}, and is shown in Fig. 4.4. During deprotection, the six-member heterocyclic ring of the acetal is converted to an aldehyde group. The oxygen atoms of the acetal moiety are not visible in the energy region available to us in multiple

internal geometry infrared spectroscopy. However, the C=O group of the aldehyde has a characteristic energy of vibration in this region. In Fig. 4.4, the red trace (*i.e.* the surface after deprotection) has a single peak centered at 1725 cm^{-1}. In comparison, the C=O bond of a neat propionaldehyde, equivalent to the aldehyde on the surface after deprotection, has a characteristic stretch vibration at 1720 cm^{-1} [11]. The position of the peak is thus consistent with the successful completion of the deprotection reaction in our experiments. The absence of any peak in this region for the acetal/methyl-terminated surfaces (*i.e.*, before deprotection) was equally important, because it showed that the deprotection occurred only after reaction with 1.0 M HCl at 80°C.

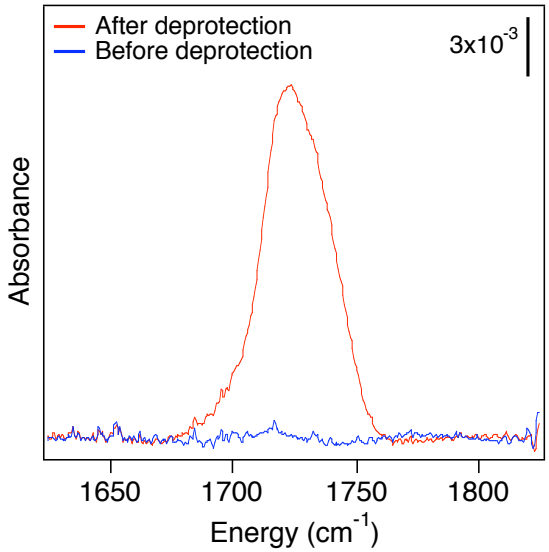

Figure 4.4 Infrared spectra for the 1,3-dioxan-2-ylethyl/methyl-terminated surface (blue trace) and the same surface after deprotection with 80°C, 1M HCl (red trace). The initial 1,3-dioxan-2-ylethyl/methyl-terminated surface was prepared using a 0.08 M 1,3-dioxan-2-ylethyl and 2.5 M methyl Grignard reagents, and the infrared data were collected in the multiple internal reflection geometry. The energy region shown corresponds to the C=O stretch.

To test whether the harsh conditions of deprotection resulted in oxidation of the surface, infrared data were collected in the transmission geometry, as shown in Fig. 4.5. The energy region studied was between 750 cm^{-1} and 1600 cm^{-1}. As in the previous figures, the blue trace in Fig 4.5 corresponds to the acetal/methyl-terminated surface and the red trace corresponds to the same surface after reaction with 1.0 M HCl at 80°C for 30 minutes. Fig. 4.5 also shows a black trace that corresponds to a surface with ~13Å of chemical-oxide. The spectrum of the chemical-oxide-terminated surface is used to as a standard for Si-O vibrational energy peaks.

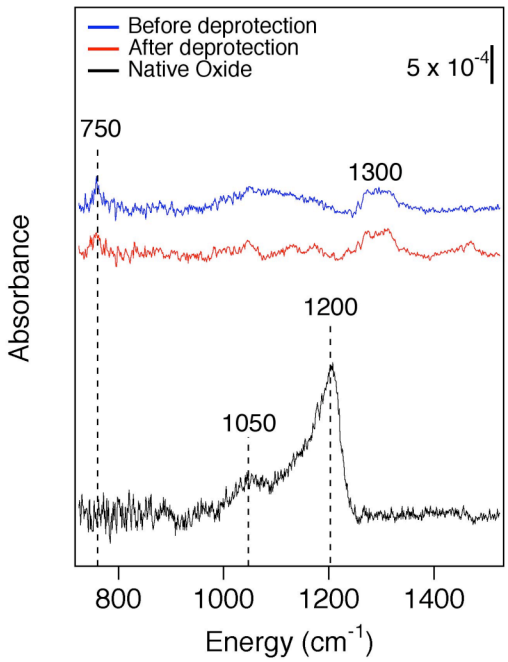

Figure 4.5 Infrared spectra collected in the transmission geometry for the 1,3-dioxan-2-ylethyl/methyl-terminated surface (blue trace) and the aldehyde/methyl-terminated surface formed after deprotection using 1.0 M HCl (red trace) in the energy region between 750 cm^{-1} and 1600 cm^{-1}. The initial 1,3-dioxan-2-ylethyl/methyl-terminated surface was prepared using a solution that was substantially 0.08 M 1,3-dioxan-2-ylethyl and 2.5 M methyl Grignard reagents. The black trace corresponds to a surface terminated with ~13 Å of chemical oxide.

The two peaks observed at 750 cm^{-1} and 1300 cm^{-1} are attributed to the rocking and umbrella modes of vibrations of CH_3 respectively [12] and is present on both red and blue spectra. This confirms the presence of methyl moieties on the surface both before and after deprotection. The black trace (*i.e.*, the chemical-oxide-terminated surface) has peaks at 1050 cm^{-1} and 1200 cm^{-1}. These two peaks correspond to the transverse and longitudinal optical Si-O vibrational bands respectively [13]. The absence of these peaks in both the red and blue spectra shows that no measurable surface oxidation occurs during functionalization.

4.3 (ii) Mechanical Properties of Mixed Acetal/Methyl-Terminated Resonators

As described earlier, the large steric bulk of the acetal group prohibited the attachment of acetal groups to each available site on the silicon surface. To determine the highest concentration of acetal functional groups that gave acceptable quality factors, we prepared a series of resonators with varying acetal/methyl ratios. In the absence of a reliable means of quantifying the relative acetal/methyl ratio on the silicon surface, we report these data in terms of the relative concentrations of acetal- and methyl-Grignard-reagent in the initial reaction mixture. These data are shown in Fig. 4.6. Although resonators terminated with pure methyl monolayers had the highest Q, the addition of ~10% acetal-Grignard-reagent led to modest (~25%) reductions in Q.

The chemical origin of the decreasing quality factor is unclear. The spectroscopic investigations described in the previous sections showed that the addition of acetal-Grignard to the reaction mixture did not lead to surface oxidation – at least on the predominant {111} faces. Interestingly, devices terminated with these

mixed acetal/methyl monolayers have comparable performance to H-terminated resonators and significantly better performance than long-chain-alkyl-terminated resonators [5]. From the standpoint of sensor production, the quality factors of the acetal/methyl-terminated resonators were entirely acceptable.

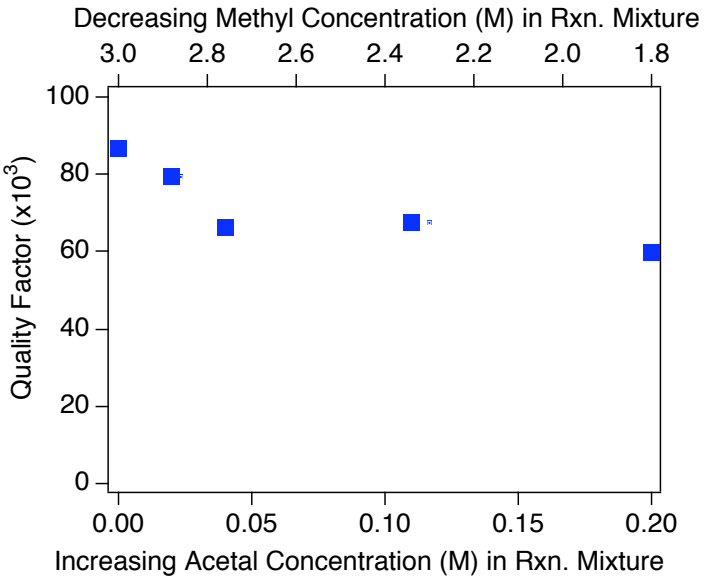

Figure 4.6 Quality factors of 5.7-μm-wide acetal/methyl-terminated resonators. The concentration of the initial reaction mixture was varied to study the change in quality factor with increasing amount of 1,3-dioxan-2-ylethyl Grignard reagent in the reaction mixture.

Acetal protecting groups can be converted to a number of common organic functionalities. In these experiments, we chose the acetal-to-aldehyde conversion as a prototypical deprotection reaction and investigated three different strategies for this transformation. In Fig. 4.7, the quality factors of mixed acetal/methyl-terminated resonators before and after deprotection in 80°C, 1 M HCl are displayed. Clearly, the harsh reaction conditions lead to a dramatic – and unacceptable – degradation of the

quality factors of the resonators. On average, this reaction led to a factor of ~5 decrease in Q.

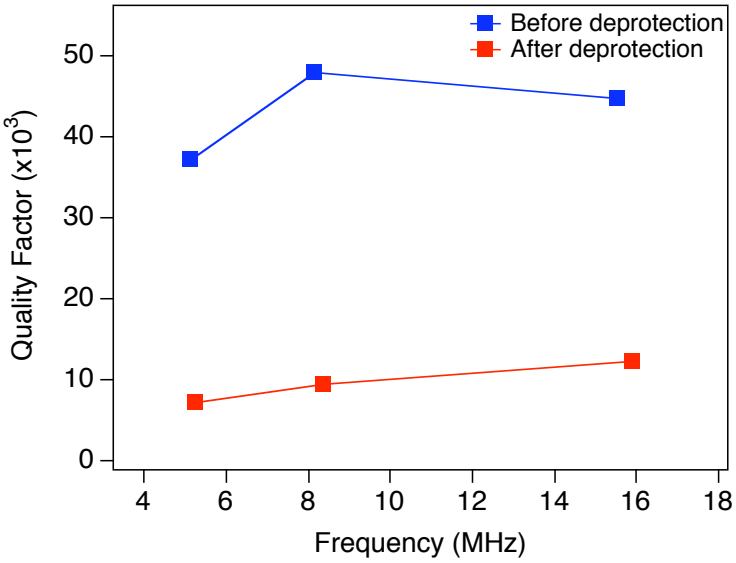

Figure 4.7 The quality factors of three different sizes of acetal/methyl-terminated resonators. The initial surface of the resonators was prepared using a mixture comprised 0.08 M 1,3-dioxan-2-ylethyl and 2.5 M methyl Grignard reagents, followed by deprotection with 80°C, 1 M HCl for 30 minutes. Although the as-prepared resonators had relatively high Q, deprotection led to a dramatic reduction in Q.

Is this dramatic quality-factor reduction driven by changes in the acetal groups or is it due to a more subtle effect? To answer this question, we performed the same "deprotection" reaction on methyl-terminated surfaces, which are expected to be unaffected by this reaction. As shown in Fig. 4.8, the hot acid treatment caused similar quality factor reductions on the methyl-terminated surface as well, suggesting that this treatment degrades the surface. The nature of this degradation in unclear, as only subtle changes (*e.g.*, no oxidation) were seen spectroscopically.

In an attempt to improve the mechanical properties of the aldehyde-terminated (*i.e.*, deprotected) resonators, a number of different deprotection strategies were also tested. In addition to varying the strong acid reaction conditions (*e.g.*, reaction time and temperature), we tried deprotection with weak acid (*e.g.*, 1.0 M acetic acid) as well as non-aqueous reaction conditions (*e.g.*, TMSI in chloroform). In all cases, a dramatic degradation upon deprotection was observed.

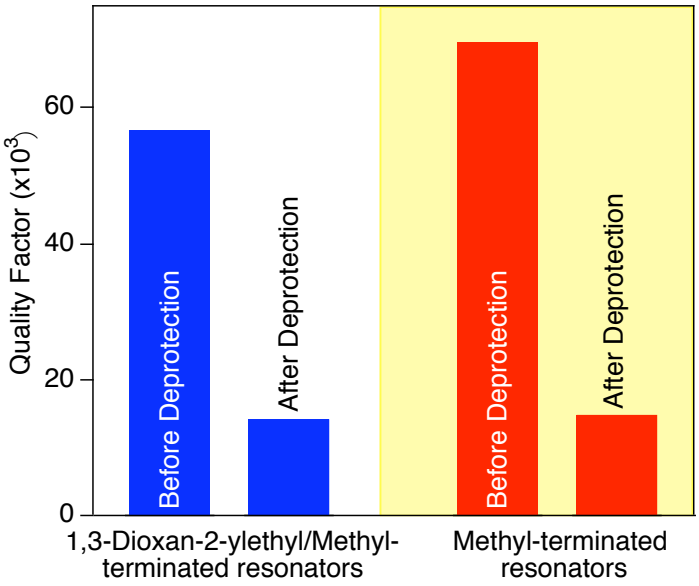

Figure 4.8 The effect of deprotection using 80°C, 1 M HCl on a 1,3-dioxan-2-ylethyl/methyl-terminated resonator, as compared to the effect of the same deprotection technique on a methyl-terminated resonator.

4.4 Discussion

In this experiment the quality of acetal/methyl-terminated resonators was found to be intermediate between methyl-terminated and long-chain-alkyl-terminated resonators. The enhanced mechanical energy dissipation in long-chain-alkyl-terminated resonators, as compared to methyl-termination, has been shown to be

correlated with the packing density of the monolayer (as discussed in Ch. 2). The acetal moiety being much larger than the methyl group, it can be assumed that the *Q* of acetal-terminated resonators would be low due to less than 50% termination of the resonator surface.

The decrease in *Q* is drastic during the transformation of the acetal to an aldehyde. Why does the deprotection chemistry result in enhanced mechanical energy dissipation? Previous results have shown that resonators terminated with ~13Å of chemical oxide showed high mechanical energy dissipation, resulting in low *Q* [14]. Since characterization of the surface after deprotection showed that there was no measurable oxidation present, an alternate explanation is required for the observed decrease in *Q* upon deprotection.

Is it possible that the harsh conditions of the deprotection reaction cause damage to the silicon layer resulting in the development of electronically active defect sites? As discussed previously in Sect. 3.4, mechanical dissipation at defect sites occurs when the material is subject to a periodic stress. As a result of the applied stress, the chemical bonds surrounding a defect site are displaced from their equilibrium position. Mechanical dissipation occurs when the relaxation time (*i.e.*, the time required by the defect site to return to equilibrium) is comparable to the vibration period of the material. In such a case, relaxation causes a significant phase lag to the applied mechanical stress, resulting in energy dissipation. (This phenomenon is described in greater detail by Braginsky *et al*. [15]) Consequently, the greater the number of defect sites, the greater would be the corresponding mechanical energy dissipation. One method that can be used to quantify electronically active defects is the measurement of charge carrier lifetimes [16]. Charge carrier lifetimes are related to

the number of defects sites, a larger number of defect sites resulting in shorter charge carrier lifetimes.

4.5 Conclusion

MHz-frequency silicon micromechanical torsional resonators were coated with mixed acetal/methyl monolayers, and the acetal groups were subsequently converted to aldehyde groups using three different synthetic strategies. Infrared absorption spectroscopy was used to verify the success of the functionalization reactions. Resonators terminated with mixed acetal/methyl monolayers had very high quality factors. In contrast, when the acetal moiety was converted to an aldehyde using standard deprotection chemistries in both aqueous and organic media, a dramatic decrease in resonator quality was observed. Spectroscopic investigations of the deprotected surfaces showed no obvious contamination or degradation. Based upon these results, acetal-based functionalization strategies appear to be poor candidates for sensor fabrication.

REFERENCES

1. T. Thundat, E. A. Wachter, S. L. Sharp, and R. J. Warmack, *Appl. Phys. Lett.* **66**, 1695 (1995).

2. T. D. Stowe, K. Yasumura, T. W. Kenny, D. Botkin, K. Wargo, and D. Rugar, *Appl. Phys. Lett.* **71**, 288 (1997).

3. R. Boukherroub, S. Morin, P. Sharpe, D. D. M. Wayner, and P. Allongue, *Langmuir* **16**, 7429 (2000).

4. M. B. Smith, and J. March, *Advanced Organic Chemistry – Reaction Mechanisms, and Structure* (Wiley, Inc. 2001).

5. Y. Wang, J. A. Henry, D. Sengupta, and M. A. Hines, *Appl. Phys. Lett.* **84**, 5736 (2004).

6. A. Bansal, X. Li, I. Lauerman, and N. S. Lewis, *J. Am. Chem. Soc.* **118**, 7225 (1996).

7. T. W. Greene and P. G. M. Wutts, *Protective Groups in Organic Synthesis*, 2nd edition (1991).

8. M. E. Jung, W. A. Andrus, and P. L. Ornstein, *Tetrahedron Lett.*, 4175 (1977).

9. W. M. Lau, L. J. Huang, W. H. Chang, M. Vos, and I. V. Mitchel, *Appl. Phys. Lett.* **63**, 78 (1993).

10. R. G. Snyder, H. L. Strauss, and C. A. Elinger, *J. Phys. Chem.* **86**, 5145 (1982).

11. C. J. Pourchert, *Aldrich Library of Infrared Spectra* (Aldrich Chem. Co., Milwaukee 1981).

12. S. Rivvilon and Y. J. Chabal, *J. Phys. IV France* **132**, 195 (2006).

13. K. T. Queeney, M. K. Weldon, J. P. Chang, Y. J. Chabal, A. B. Gurevich, J. Sapjeta, and R. L. Opila, *J. Appl. Phys.* **87**, 1322 (2000).

14. W. J. Royea, A. Juang, and N. S. Lewis, *Appl. Phys. Lett.* **77**, 1988 (2000).

15. V. B. Braginsky, V. P. Mitranov, and V. I. Panov, *Systems with Small Dissipations* (University of Chicago Press, Chicago 1985).

16. E. Yablonovitch, D. L. Allara, C. C. Chang, T. Gmitter, and T. B. Bright, *Phys. Rev. Lett*. **57**, 249 (1986).

Chapter 5

Functionalizing Silicon Resonators Using Olefin Cross-Metathesis Reactions

5.1 Introduction

Micromechanical resonators can potentially be used as chemical and biological sensors; however, the utility of a sensor is limited by its ability to selectively react with the analyte of interest. To enable reaction of the resonator surface with a particular analyte, the surface has to be terminated with functional groups selective towards that analyte. In these studies, our goal was to develop a platform surface functionalization strategy that would protect the silicon surface from degradation while also allowing the attachment of any desired reactive functionality. As shown by the previous chapter, functionalized silicon resonators are irreversibly damaged by harsh reaction conditions, so a mild, room temperature method requiring minimum exposure to organic solvents was sought.

Olefin cross-metathesis reaction using the Grubbs catalyst seemed to be an ideal fit to these requirements. In olefin cross-metathesis, terminal alkene groups on two different molecules undergo a catalyzed reaction that results in the formation of a single alkene bond. The beauty of the Grubbs catalyst lies in its high selectivity towards the terminal alkene bond, even in the presence of other functional groups. Furthermore, the initial terminal alkene could be readily prepared using Grignard reagents – an approach that had been previously shown to give high quality resonators. During our exploration into the feasibility of this approach, Yang *et. al.* [1] reported a similar method for the functionalization of silicon surface, using olefin metathesis chemistry, which we adapted for our experiment.

In the following, we demonstrate the feasibility of the strategy using a prototypical system – the production of ester-functionalized resonators. Resonators functionalized with mixed butenyl/methyl monolayers were chosen as the starting point for the synthesis. The small methyl groups allowed for the functionalization of essentially every site on the surface, whereas the butenyl groups provided the necessary terminal double bond for the olefin cross-metathesis. The butenyl groups were chosen to be long enough to sit well above the methyl "carpet" but not long enough to allow collapse onto the surface.

5.2 Experimental

As described in Ch. 2, double-clamped, MHz-frequency, single-crystal silicon resonators were fabricated using lithographic techniques. The resonators consisted of a central hexagonal paddle connected to the bulk by two 440-nm-wide, 4-μm-long supporting beams. Three different paddle widths were studied, measuring 4.2 μm, 5.7 μm and 7.2 μm across the flats. The paddles and supporting beams had the same thickness, which varied over the range 350-425 nm depending on the final etch duration. The resonant frequencies of the paddles depended on both their size and thickness; they varied over the range of 4-17 MHz. Depending on size, 74-87% of the exposed surface was composed of {111} faces. An SEM of a typical resonator is shown in Fig 2.1.

The resonators were first hydrogen-terminated, as described in Sect. 2.2(v), placed in a quartz round-bottom flask and attached to a Schlenk line. The resonators were then Cl-terminated, as described in Sect. 2.4(ii). A reaction mixture that was simultaneously 0.3M in 3-butenyl Grignard reagent (C_4H_7MgBr, 0.5 M in THF, Sure-Seal, Aldrich) and 1.2M in methyl Grignard reagent (CH_3MgCl, 3.0 M in THF, Sure-

Seal, Aldrich) was measured into a graduated cylinder attached to the Schlenk line under a constant flow of Ar. A double-tipped needle was then used to cannulate the reagent mixture into the flask containing the Cl-terminated resonators under a positive pressure of Ar. The samples were left to react with the Grignard reagent mixture for 1.5 hours under reflux conditions (~67°C) under a constant flow of Ar. At the end of the reaction, the reagent mixture was diluted with THF and decanted, followed by rinsing of the resonators with anhydrous methanol, dichloromethane and ultrapure water.

The terminal alkene on the butenylated-resonator was reacted with the terminal alkene on the ethyl 10-undecenoate molecule. To prevent the reaction between terminal alkenes on two ethyl 10-undecenoate molecules, the cross-metathesis reaction was carried out in two steps with through rinsing of the resonators between the two steps. In the first step, a 13 mM solution of 1st generation Grubbs' catalyst ($C_{43}H_{72}Cl_2P_2Ru$, Aldrich) in chloroform was prepared as described in Sect. 2.4(iii). The catalyst solution was then transferred into the flask containing the butenyl/methy-terminated resonators and left to react for 30 min at room temperature under a constant flow of Ar. After the reaction, the resonator samples were rinsed sequentially with methylene chloride and ultrapure water. In the second step, the catalyst-coated samples were placed in a clean round-bottom flask, and enough neat ethyl 10-undecenoate ($C_{13},H_{24}O_2$, >97%, Aldrich) was added to the flask to completely cover the sample. The flask was then attached to a Schlenk line, the ethyl 10-undecenoate degassed, and the samples left under a constant flow of Ar for 30 min at room temperature. The samples were then rinsed in methylene chloride and ultrapure water. Due to the high viscosity of the ethyl 10-undecenoate, copious rinsing was required.

For comparison purposes, methyl-terminated resonators were prepared by reacting Cl-terminated resonators with methyl Grignard reagent. In this experiment, methyl Grignard reagent was cannulated into a round-bottom flask containing Cl-terminated resonators, the preparation of which has been described in Sect. 2.4(ii), under a positive pressure of Ar. The resonators were refluxed at ~67°C in the methyl Grignard reagent for 1.5 hours under a constant flow of Ar. At the end of the reaction, the reagent was diluted with THF, and the samples rinsed with anhydrous methanol, methylene chloride and ultrapure water. To test the effects of the metathesis reaction on methyl-terminated surfaces, the methyl-terminated resonators were exposed to Grubbs' catalyst and ethyl 10-undecenoate under the same reaction conditions as described above for the butenyl/methyl-terminated resonators.

After surface functionalization, the samples were either loaded into a vacuum chamber for mechanical property measurements or into an FTIR spectrometer for surface characterization.

5.3 Results

The chemical composition of the functionalized surfaces was studied using both infrared and X-ray photoelectron spectroscopy. The infrared spectra were collected in both the multiple-internal-reflection (MIR) and transmission geometries. Due to their extremely small size, direct characterization of the resonator surface was not possible. Instead, 0.59″×1.56″ Si(111) samples, processed simultaneously with the resonator samples, were characterized. For MIR measurements, the shorter sides of these silicon samples were beveled at 45° as described in Sect 2.5(i).

5.3 (i) Characterization of the Methyl/Butenyl Si(111): Effect of Olefin Cross-Metathesis

Figure 5.1 shows infrared absorption spectra for a butenyl/methyl-terminated surface and a methyl-terminated surface before (blue trace) and after (red trace) the olefin cross-metathesis reaction. The methyl-terminated surface was used as a control in this experiment to confirm that the metathesis reaction does not occur in the absence of an alkene. The metathesis experimental conditions used on the methyl-terminated surface was identical to those for the butenyl/methyl-terminated surface and are described in detail in Sect. 5.2.

There are two energy regions shown in Figure 5.1. The first, between 1600 cm^{-1} and 1850 cm^{-1}, corresponds to the energy region which is characteristic of C=O stretch vibrations. The second energy region, between 2700 cm^{-1} and 3100 cm^{-1}, corresponds to C–H stretch vibrations. Before olefin cross-metathesis, the Si(111) surface is terminated with a mixture of CH_3 moieties and alkyl moieties with a terminal double bond. After cross-metathesis between the terminal alkene bonds on the Si(111) surface and the terminal alkene bond on the 10-undecanoate moieties, the surface should be terminated with a mixture of methyl and ester moieties. The additional of ester moieties to the silicon surface results in C=O and C–O bonds. In the energy region available when using multiple internal reflection geometry, the vibration of the C–O species is not observable. However, the C=O group on the ester has a characteristic stretch vibration between 1730 cm^{-1} and 1750 cm^{-1} [5], depending on the chemical environment. In Fig. 5.1, a peak is observed at 1733 cm^{-1} for the butenyl/methyl-terminated surface only after the olefin cross-metathesis reaction. This peak can be attributed to the carbonyl species of the ester, which confirms the presence of ethyl 10-tridecenoate moieties at the silicon surface

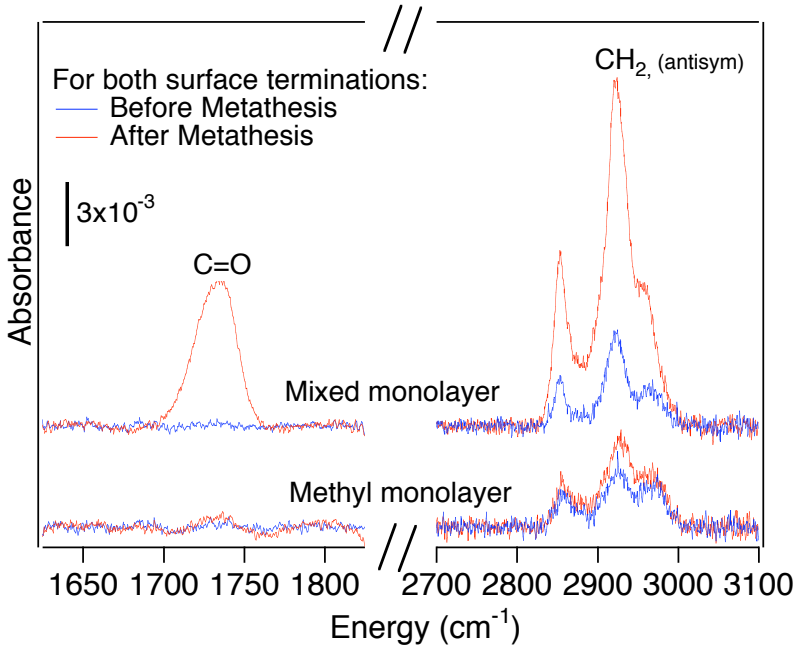

Figure 5.1 Infrared absorption spectra collected in multiple internal reflection geometry for a butenyl/methyl-terminated Si(111) surface. The blue and red traces correspond to the functionalized surface before and after olefin cross-metathesis respectively. The lower energy region, between 1650 cm^{-1} and 1850 cm^{-1}, corresponds to C=O stretch vibrations, and the higher energy region, between 2700 cm^{-1} and 3100 cm^{-1} corresponds to C–H stretch vibrations. The appearance of a peak at approximately 1733 cm^{-1} signifies the success of the metathesis reaction.

The higher energy region shown in Fig. 5.1 corresponds to C-H stretch vibrations. The infrared spectra corresponding to the surface terminated with butenyl/methyl surfaces both before and after olefin cross-metathesis show absorption peaks between 2700 cm^{-1} and 3100 cm^{-1}, confirming the presence of CH_2 groups on the silicon surface. For alkyl-terminated surfaces, the position of the antisymmetric CH_2 stretch vibration is a good indicator of the quality of the monolayer on the surface as a result of its sensitivity towards the density of the monolayer. A shift of approximately 6-8 cm^{-1} to higher energies has been observed in the position of this antisymmetric CH_2 peak during the crystallization of liquid alkanes [6]. In alkyl-

terminated monolayers, this shift to higher energies is associated with the decrease in the ordering in the monolayer, resulting in a more liquid-like arrangement.

The antisymmetric CH_2 stretch vibration for the butenyl/methyl-terminated surface (*i.e.*, the blue trace) lies at 2924 cm^{-1}. After olefin cross-metathesis is performed on the methyl/butenyl-terminated surface, the antisymmetric CH_2 peak shifts from 2924 cm^{-1} to 2922 cm^{-1}. The shift of the antisymmetric CH_2 peak by 2 cm^{-1} to a lower energy indicates that there is a change in the quality of the butenyl/methyl mixed monolayer as a result of the metathesis reaction. Another significant difference between the blue and the red trace is the intensity of the peaks. The intensity of the peaks increases after olefin cross-metathesis. This further indicates that the reaction is a success. After olefin cross-metathesis between the terminal alkene on the surface butenyl and the terminal alkene on the ethyl undecanoate molecule, the C-H bonds are added to the silicon surface, increasing the intensity of the C-H stretch peaks. For the methyl-terminated surface, no change is observed either in the position or intensity of the antisymmetric CH_2 peak, indicating that the metathesis reaction does not affect the chemical bonds on the silicon surface.

The effect of the metathesis reaction on a methyl-terminated surface was also characterized using infrared spectroscopy. In Fig. 5.1, the lower red and blue spectra correspond to the methyl-terminated surface before (blue trace) and after (red trace) exposure to the metathesis reaction conditions. There is no perceptible change in the spectra before and after exposure to the metathesis reaction conditions for the methyl-terminated surface. This demonstrates that metathesis does not take place in the absence of the terminal alkene of the butenyl/methyl-terminated surface.

To test whether the metathesis reaction resulted in the formation of surface oxide, infrared data was collected in the transmission geometry. In Fig. 5.2, the blue

trace corresponds to a butenyl/methyl-terminated surface before metathesis, the red trace corresponds to the same surface after metathesis, and the black trace corresponds to a chemical oxide-terminated surface. The peaks at 750 cm^{-1} and 1250 cm^{-1} observed for the butenyl/methyl-terminated surface, both before and after metathesis, are attributed to the rocking and umbrella modes of vibration of CH_3 respectively [8], indicating the presence of methyl moieties.

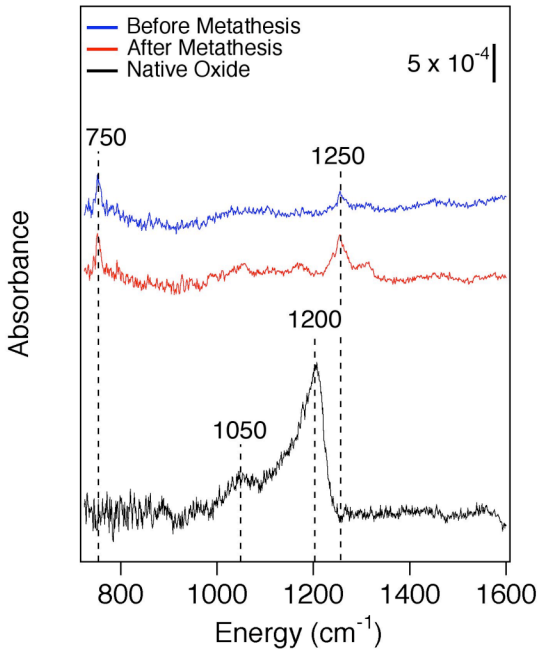

Figure 5.2 Infrared spectra collected in the transmission geometry. The three spectra correspond to the butenyl/methyl-terminated surface before (blue trace) and after (red trace) olefin cross-metathesis, and a surface terminated with ~13Å of chemical oxide (black trace.)

The peaks at 1000 cm^{-1} and 1250 cm^{-1} observed in the spectrum of the oxidized surface are due to transverse and longitudinal optical modes of the Si–O stretch respectively [9]. The absence of these peaks in the spectra of the butenyl/methyl-terminated surface both before and after metathesis shows that no observable oxidation occurs as a result of olefin cross-metathesis.

5.3 (ii) X-Ray Photoelectron Spectroscopy

Butenyl/methyl-terminated surfaces were further characterized using X-ray photoelectron spectroscopy. This experiment was performed to confirm that after metathesis, no residual Grubbs' catalyst remained on the functionalized silicon surface. The presence or absence of ruthenium peaks in the XPS spectrum was used to characterize the presence of residual Grubbs' catalyst on the functionalized silicon surface.

Figure 5.3 is a survey scan characterizing the butenyl/methyl-terminated surface after metathesis. The silicon peaks are due to the silicon substrate, and the carbon peak is due to the organic monolayer on the silicon surface. The survey scan also shows an oxygen transition at ~520 eV, which is attributed to contamination during sample introduction and pump down. The black circle indicates the binding energy of Ru($3p_{3/2}$) and Ru($3p_{1/2}$) electrons [10]. The absence of peaks corresponding to the ruthenium core electrons shows that there is no residual Grubbs' catalyst remaining on the surface after the completion of the metathesis reaction.

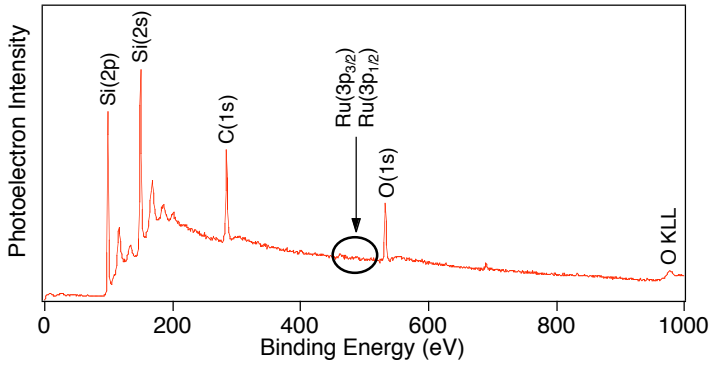

Figure 5.3 X-Ray Photoelectron Spectroscopy survey scan for silicon surface terminated with a mixture of butenyl and methyl moeities on which the metathesis reaction has been carried out. The absence of Ru core electrons shows that there is no residual Grubbs' catalyst at the completion of the metathesis reaction.

XPS was also used to characterize any surface oxidation that may have resulted from the metathesis reaction. Figure 5.4 shows high resolution spectra specific to the Si (2p) core electrons. The high resolution scan can be used to detect the presence of silicon sub-oxides (*e.g.*, Si^{1+}, Si^{2+}, Si^{3+}.) These sub-oxide species have energies at 100.9 eV, 102.0 eV and 103.1 eV, respectively [11]. In Fig 5.4, the red trace corresponds to a butenyl/methyl-terminated surface after metathesis. The blue trace corresponds to an oxidized silicon sample, with a peak appearing at ~102.7 eV is close to the 103.1eV peak reported for Si_2O_3 [11]. This peak is absent on the blue trace, thus indicating the no observable oxidation occurs at the silicon surface during metathesis.

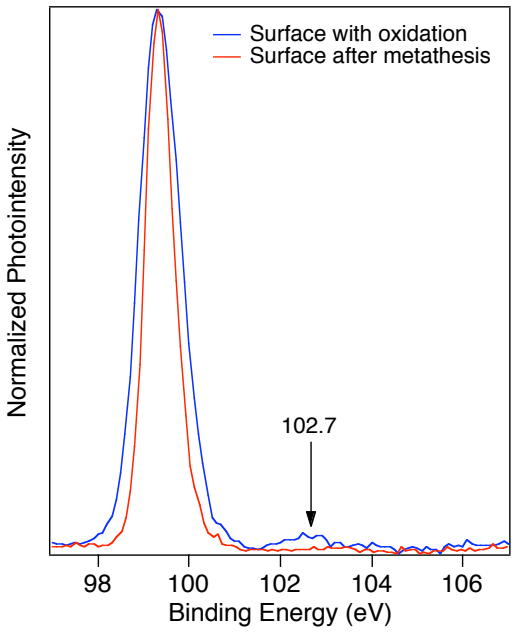

Figure 5.4 X-Ray Photoelectron Spectroscopy showing a high resolution Si (2p) scan of the butenyl/methyl-terminated surface (red trace) after metathesis. The blue trace is a high resolution scan of a Si(111) surface that has been oxidized. The silicon oxide peak is at ~102.7 eV.

5.3 (iii) Mechanical Properties of Mixed Butenyl/Methyl-Terminated Resonators: The Effect of Olefin Cross-Metathesis on High *Q* Resonators

The effect of olefin cross-metathesis on butenyl/methyl-terminated resonators was studied by measuring the mechanical property of the resonators. The *Q* for the butenyl/methyl-terminated resonators was measured both before and after metathesis. As a control experiment, the effect of metathesis reaction on methyl-terminated resonators on *Q* was simultaneously studied. The results of these experiments are shown in Fig. 5.5 for the case of 5.7-μm-wide resonators. The *Q* of butenyl/methyl-terminated resonators is comparable to the *Q* of methyl-terminated resonators [2]. After olefin cross-metathesis is performed on the butenyl/methyl-terminated resonators, the *Q* decrease by ~50% as compared to the initial *Q* of butenyl/methyl-terminated resonators. This *Q* is comparable to that of similar long-chain-alkyl-terminated resonators [3]. Interestingly, methyl-terminated resonators exposed to the olefin-metathesis reaction conditions displayed a similar decrease in *Q*. This result shows that it is not the metathesis reaction itself that decreases the *Q* of functionalized resonators, but it is the reaction conditions that contribute to the degradation of the mechanical property of the resonators.

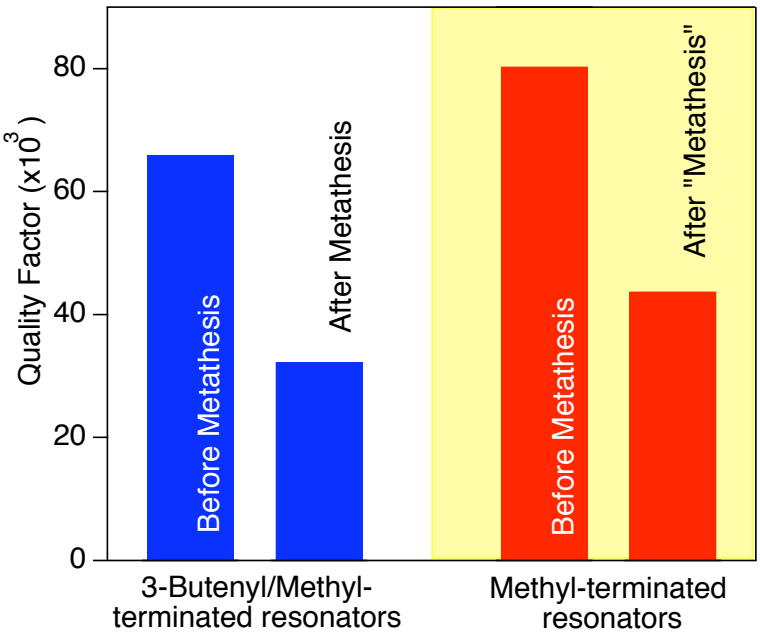

Figure 5.5 The effect of metathesis reaction conditions on the quality factor of butenyl/methyl- and purely methyl-terminated resonators. Data on the left (white background) are for metathesis performed on 5.7-μm-wide butenyl/methyl-terminated resonators, and data on the right (yellow background) are for the same reaction performed on 5.7-μm-wide methyl-terminated resonators. The mixed-monolayer-terminated resonators were prepared using reaction mixture that was simultaneously 0.3 M in 3-butenyl Grignard reagent and 1.2 M in methyl Grignard reagent.

5.3 (iv) Long-Term Stability of Mixed Ester/Methyl-Terminated Resonators

The long-term stability of resonators functionalized using olefin cross-metathesis was also studied. In this experiment, the functionalized resonators were stored in vacuum (~10^{-8} Torr) and the *Q*'s measured periodically over the course of 69 hours. The resonators were then stored in room air at 100% humidity in a bell jar for an additional 70 hours. The resonators were then re-loaded into the vacuum chamber and the mechanical properties measured. The quality factors of 4.2-um-wide resonators are shown as a function of time in Fig. 5.7. (Other resonator sizes showed

similar trends.) The value of Q remains consistent over the first 69 hours with an average Q of ~ 35000. A decrease of ~15% from the average Q (for the first 69 hours in vacuum) is observed after exposure to 100% humidity for 70 hours.

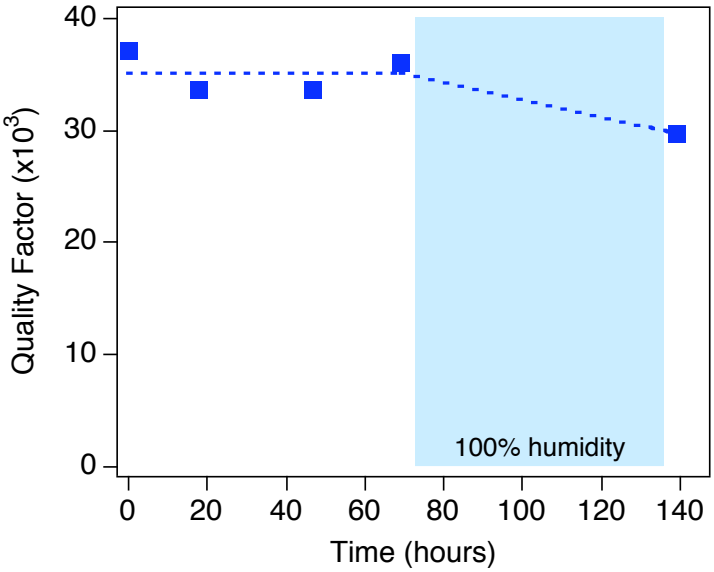

Figure 5.7 The change in quality factor of 4.2-μm-wide ester/methyl-terminated resonators over time. For the first 69 hours the resonators were stored at 10^{-8} Torr followed by exposure to 100% humidity for 70 hours (shaded region). The quality factor was relatively constant in vacuum, with a 15% decrease after exposure to 100% humidity. All measurements were made at 10^{-8} Torr.

5.4 Discussion

These experiments strongly suggest that olefin cross-metathesis reactions catalyzed by the 1st generation Grubbs' catalyst may be used as viable platform chemistry for the functionalization of micro- and nano-mechanical resonators. Infrared absorption spectroscopy showed that this reaction formed the desired functionalities on the surface, at least for ester-terminated surfaces. Importantly, this reaction did not lead to any observable oxidation of the underlying silicon surface as confirmed by

infrared spectroscopy. Furthermore, XPS measurements showed that the metathesis proceeded to completion, as no Ru-containing catalyst was observed on the surface after the reaction. In addition to functionalizing the surface, this reaction did not have a significantly deleterious effect on the mechanical properties of the resonators. Although a small (~50%) decrease in quality factor was observed, this small decrease should be acceptable for most applications. Additionally, the functionalized resonators were stable in both vacuum and 100% humidity.

The beauty of the olefin cross-metathesis reaction is its near-universal applicability. In principle, any functional group that can be attached to an alkyl chain with a terminal double bond can be attached to the initial butenyl/methyl-terminated surface by olefin cross-metathesis. Furthermore, there is good reason to believe that this reaction will not have a deleterious effect on quality factor. Though the effect on mechanical energy dissipation has only been tested in the case of the ethyl 10-undecenoate molecule, the control reaction on methyl-terminated resonators shows that the observed small decrease in Q is not due to the metathesis reaction or the attached molecule itself. One application that will be studied in the near future is functionalization of resonators with a dimethoxy-phenyl group. The dimethoxy-phenyl group should selectively bind to dinitrotoluene (DNT) – a contaminant in most commercial sources of trinitrotoluene (TNT). If so, resonators functionalized with this group may be useful to the detection of TNT-based explosives.

The olefin cross-metathesis reaction should also be readily amenable to the production of multi-functionalized chips. For example, a chip with many resonators could first be functionalized with a butenyl/methyl coating and then activated over its entire surface with the catalyst solution. Ink-jet printing techniques could then be used to pattern different regions of the chip (*i.e.*, different resonators) with different

functional groups. Importantly, this strategy could also be used to produce unfunctionalized resonators in a functionalized chip. The combination of both functionalized and unfunctionalized resonators on the same chip would be useful for both high sensitivity measurements (*i.e.*, by allowing for *in-situ* temperature correction) as well as for the detection of non-specific binding events.

5.5 Conclusion

In this experiment, the mechanical properties of butenyl/methyl-terminated resonators were measured and were found to be comparable to those observed for high *Q* methyl-terminated resonators. It was also demonstrated that the terminal alkene of butenyl moieties could successfully react with a terminal alkene on ethyl 10-undecenoate molecules via olefin cross-metathesis, resulting in surfaces terminated with ester moieties. The *Q* of butenyl/methyl-terminated resonators decreases after metathesis. This decrease in *Q* is acceptable. Furthermore, the ester/methyl-terminated resonators are stable over time in vacuum, and in 100% humidity. The olefin cross-metathesis reaction is therefore a successful method for direct functionalization of resonators surfaces with various functional groups without compromising the quality of the resonators.

REFERENCES

1. L. Yang, Y.-Y. Lua, O. A. Scherman, R. H. Grubbs, J. N. Harb, R. C. Davis, M. R. Linford, *Chem. Mater*. **19**, 1671 (2007).

2. Y. Wang, J. A. Henry, D. Sengupta, and M. A. Hines, *Appl. Phys. Lett.* **85**, 5736 (2004).

3. J. A. Henry, Y. Wang, and M. A. Hines, *Appl. Phys. Lett.* **84**, 1765 (2004).

4. W. M. Lau, L. J. Huang, W. H. Chang, M. Vos, and I. V. Mitchel, *Appl. Phys. Lett.* **63**, 78 (1993).

5. D. A. Skoog, F. J. Holler, and T. A. Nieman, *Principles of Instrumental Ananlysis*, 5th Ed. (1998).

6. R. G. Snyder, H. L. Strauss, and C. A. Elinger, *J. Phys. Chem.* **86**, 5245 (1982).

7. M. R Linford, P. Fenter, P. M. Eisenberger, and C. E. D. Chidsey, *J. Am. Chem. Soc*. **117**, 3145 (1995).

8. S. Rivillon and Y. J. Chabal, *J. Phys. IV France* **132**, 195 (2006).

9. K. T. Queeney, M. K. Weldon, J. P. Chang, Y. J. Chabal, A. B. Gurevich, J. Sapjeta, and R. L. Opila, *J. Appl. Phys.* **87**, 1322 (2000).

10. J. F. Moulder, W. F. Stickle, P. E. Sobol, and K. D. Bomben, *Handbook of Photoelectron Spectroscopy* (Physical Electronics Division, 1992).

11. F. J. Grunthaner, P. J. Grunthaner, R. P. Vasquez, B. F. Lewis, and J. Maserjian, *Phys. Rev. Lett.* **43**, 1683 (1979).

12. Y. Wang, J. A. Henry, A. T. Zehnder, and M. A. Hines, *J. Phys. Chem. B* **107**, 14170 (2003).

13. P. T. Hurley, E. J. Nemanick, B. S. Brunschwig, and N. S. Lewis, *J. Am. Chem. Soc*. **128**, 1990 (2006).

14. H. C. Kolb, M. G. Finn, and B. K. Sharpless, *Angew. Chem. Int. Ed.* **40**, 2004 (2001).